12. Orbital and Spin Magnetism. Fine Structure

12.1 Introduction and Overview

We have not yet discussed the magnetic properties of atoms. It turns out that the study of these properties yields a deeper insight into the shell structure of atoms.

The impetus to study the magnetic properties was given by a few fundamental experiments, which we shall discuss in this chapter. The most important are

- Measurements of the macroscopic magnetisation and of the gyromagnetic properties of solids, known as the Einstein-de Haas effect.
- Measurements of directional quantisation and of the magnetic moments of atoms in atomic beams, made by *Stern* and *Gerlach*.
- Observation of the so-called fine structure in the optical spectra of atoms.

We shall begin with the third point. Many of the lines in the spectra of alkali atoms are double, and are called doublets. They occur because all the energy terms $E_{n,l}$ of atoms with single valence electrons, except for the s terms (energy levels with no orbital angular momentum), are split into two terms. This splitting cannot be understood in terms of the theory discussed so far. It is fundamentally different from the lifting of orbital degeneracy discussed in the last chapter. If the orbital degeneracy has already been lifted, there must be a new effect involved, one which has not yet been taken into account. Let us take as an example the D line in the spectrum of the sodium atom, i.e. the transition $3P \leftrightarrow 3S$ (Fig. 11.7 and 12.1). With sufficient spectral resolution, one can see two lines: $D_1 = 589.59$ nm $\triangleq 16956$ cm^{-1} and $D_2 = 588.96$ nm $\triangleq 16973$ cm^{-1}. In the following we shall often use this pair of lines as an example for explanation and experimental demonstration of spectroscopic results. Like the Balmer series of the H atom, the sodium D lines are especially suitable for demonstration of basic concepts in atomic spectroscopy – so much so, that they have become the "guinea pigs" of the field.

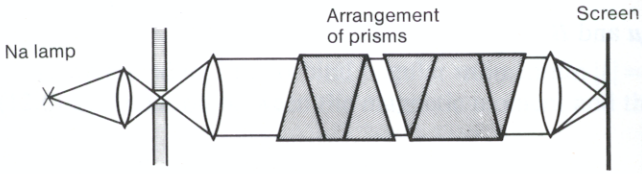

Fig. 12.1. Arrangement for spectral separation of the two components D_1 and D_2 of the sodium D line. With this arrangement, the splitting can easily be demonstrated in the lecture hall by replacing the screen with a television camera. To separate the lines distinctly, one needs two commerically available straight-through prisms

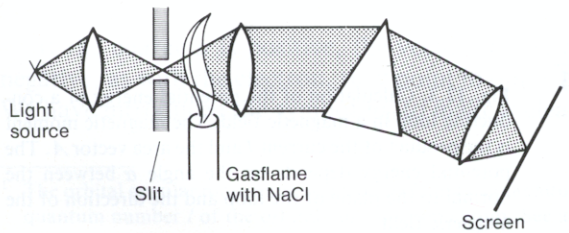

Fig. 12.2. Arrangement for observation of the sodium D lines by absorption (as the so-called Fraunhofer line). The continuous spectrum of an arc lamp or xenon high-pressure lamp is spread out by a prism. A gas flame made yellow by addition of NaCl, or better still, sodium vapour from a heated piece of sodium metal, absorbs the light of the D line from the continuous spectrum. On the screen, therefore, the line is seen as a black band on the continuous spectrum

To explain the doublet structure, one needs three additions to our previous picture:
- A *magnetic moment* μ_l is associated with the orbital angular momentum l.
- The electron also has a *spin* s. It too is associated with a magnetic moment, μ_s.
- The two magnetic moments μ_s and μ_l interact. They can be parallel or antiparallel to each other. The two configurations have slightly different binding energies, which leads to the *fine structure* of the spectrum.

Two demonstrations of the yellow sodium lines are shown in Figs. 12.1 and 12.2; other experiments follow in Chap. 13.

12.2 Magnetic Moment of the Orbital Motion

An electron moving in an orbit is equivalent to a circular electric current. We know from electrodynamics that a circular electric current generates a magnetic dipole field. We expect that the orbiting electron will do the same, and it does in fact have a magnetic dipole moment. This we shall now calculate.

The magnetic dipole moment of a conducting loop is defined as

$$\mu = I \cdot A \quad [\mathrm{Am}^2], \tag{12.1}$$

where I is the current, and A is a vector which is perpendicular to the plane of the conducting loop and which has a magnitude equal to the area enclosed by the loop. Thus the vector μ is also perpendicular to the plane of the loop.

If we bring this magnetic dipole into a homogeneous magnetic field B, a torque τ is applied to the dipole:

$$\tau = \mu \times B\,. \tag{12.2}$$

The magnetic potential energy of the dipole is (Fig. 12.3)

$$V_{\mathrm{mag}} = -\mu \cdot B = \int_{\pi/2}^{\alpha} \tau \, d\alpha = -\mu B \cos\alpha\,, \tag{12.3}$$

where α is the angle between μ and B.

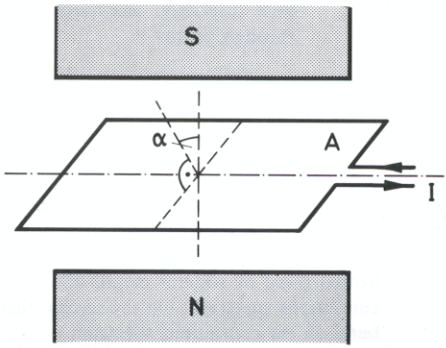

Fig. 12.3. Calculation of the potential energy of a conducting loop in a magnetic field. The magnetic moment is the product of the current I and the area vector A. The potential energy depends on the angle α between the normal to the plane of the loop and the direction of the magnetic field

The magnetic moment can be defined either in terms of the torque in the field (12.2) or the potential energy (12.3).

In atomic and nuclear physics, the magnetic moment is often defined as the torque in a uniform field of strength H (not of strength B). Accordingly,

$$\tau = \mu' \times H\,, \qquad \mu' = \mu_0 I A\,, \tag{12.4}$$

if we indicate magnetic moments which are defined w.r.t. H by μ'. Because of the relation $B = \mu_0 H$, the induction constant $\mu_0 = 4\pi \cdot 10^{-7}$ Vs/Am occurs in (12.4).

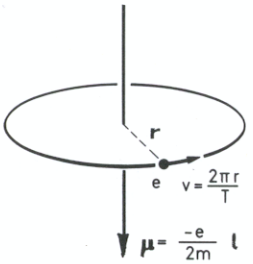

Fig. 12.4. Calculation of the orbital moment. The circulating electron has an angular momentum l and a magnetic dipole moment μ_l. For a negative charge, the vectors l and μ_l point in opposite directions

We now wish to transfer the definition of the magnetic dipole moment to the atom and calculate the magnetic moment of an electron with the charge $q = -e$ which is in a circular orbit moving with the velocity v (Fig. 12.4). If the time for a single revolution is $T = 2\pi/\omega$, a current

$$I = \frac{q}{T} = -\frac{e\omega}{2\pi} \tag{12.5}$$

is flowing. Here we have used e (without a sign) for the elementary unit of charge. Here and in the following, we use a negative sign for the electron.

The magnetic moment μ of this circular current is then, according to (12.1),

$$\mu = IA = -\tfrac{1}{2} e\omega r^2\,. \tag{12.6}$$

If we introduce[1] the orbital angular momentum $|l| = mvr = m\omega r^2$, we can rewrite (12.6) as a relation between the magnetic moment and the orbital angular momentum

$$\mu = -\frac{e}{2m_0} l\,. \tag{12.7}$$

If the charge q is positive, the vectors μ and l point in the same direction; if it is negative, as with the electron, they point in opposite directions. Therefore (12.7) holds. We have introduced the symbol m_0 to make it clear that the rest mass is what is meant.

---

[1] The orbital angular momentum is given by l, and its magnitude by $|l|$. This is to prevent confusion with the quantum number l of the orbital angular momentum. See also (8.28)

The proportionality between angular momentum and magnetic moment is also known as the magnetomechanical parallelism. The fact that it is valid in atoms is by no means self-evident, and follows from experimental observations which will be discussed below.

As the unit of magnetic moment in atoms, we use the strength of the moment which corresponds to an electron with the orbital angular momentum $|\boldsymbol{l}| = h/2\pi$. This is the orbital angular momentum in the first Bohr orbit of the hydrogen atom in the old Bohr model. An electron with $|\boldsymbol{l}| = h/2\pi$ or $\hbar$ produces a magnetic moment given by the *Bohr Magneton*:

$$\mu_B = \frac{e}{2m_0}\hbar = 9.274078 \cdot 10^{-24}\,\mathrm{Am}^2 . \tag{12.8}$$

It is an unfortunate – but, because of its wide usage, unavoidable – inelegance that the same symbol μ is used both for the magnetic moments μ and μ_B and for the induction or permeability constant of vacuum, μ_0.

The magnetic moments of electrons are frequently given in units of μ_B. For the magnitude of the magnetic moment of an orbit with the angular momentum quantum number l, the following expression is valid:

$$\mu_l = \mu_B\sqrt{l(l+1)} = \frac{e}{2m_0}\hbar\sqrt{l(l+1)} . \tag{12.9}$$

This expression is also valid for vectors, in the form

$$\boldsymbol{\mu}_l = -g_l\mu_B\frac{\boldsymbol{l}}{\hbar} . \tag{12.10}$$

Equation (12.10) thus defines the g factor, which we shall often meet in the following. It is dimensionless and here has the numerical value $g_l = 1$. It is a measure of the ratio of the magnetic moment (in Bohr magnetons) to the angular momentum (in units of $\hbar$). It was introduced by Landé, in the presence of spin-orbit coupling (Sects. 12.7, 8), in order to characterise the ratio of the magnetic moment (in μ_B) and the total angular momentum (in units of $\hbar$).

With "angular momentum", we often denote – briefly but inaccurately – the quantum number l, i.e. the maximum component in the z direction, $l_z/\hbar$. The maximum component of μ in the z direction is then given by $(\mu_z)_{max} = g_l l\mu_B$. We will treat the g factors for other cases of the angular momentum later. They are always defined as the ratio of the magnetic moment to the corresponding angular momentum, in units of μ_B and $\hbar$, respectively.

12.3 Precession and Orientation in a Magnetic Field

An applied field with the magnetic flux density $\boldsymbol{B}_0$ acts on the orbital magnetic moment $\boldsymbol{\mu}_l$ by trying to align the vectors $\boldsymbol{\mu}_l$ and $\boldsymbol{B}_0$ parallel to one another, since the potential energy is a minimum in this orientation (12.3). The electrons, which are moving in their orbits, behave mechanically like gyroscopes and carry out the usual preces-

sion about the direction of the field. The precession frequency ω_p of a gyroscope under the action of a torque τ is

$$\omega_p = \frac{|\tau|}{|l| \sin \alpha}, \tag{12.11}$$

where l is the angular momentum of the gyroscope, and α the angle between the directions of l and B_0 (Fig. 12.5).

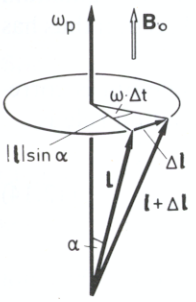

Fig. 12.5. Vector diagram for the calculation of the precession frequency ω_p of a gyroscope with angular momentum l and magnetic moment μ. The angle between the field B_0 and the direction of l (and μ) is denoted by α; the vectors Δl and τ are perpendicular to l and B

These considerations may be directly transferred to the case of the atomic gyroscope. The precession frequency of the electron orbit, the *Larmor frequency*, is found from (12.10) and (12.11) to be

$$\omega_L = \frac{|\tau|}{|l| \sin \alpha} = \frac{\mu_l B \sin \alpha}{|l| \sin \alpha} = \frac{g_l \mu_B}{\hbar} B = \gamma B . \tag{12.12}$$

The new quantity γ which we have introduced here is called the *gyromagnetic ratio*. It gives the precession frequency in a field with a magnetic flux density of 1 $Vs/m^2 = 1$ tesla. The sign and direction of the vectors is indicated in Fig. 12.6. As can be seen from (12.12), the Larmor frequency ω_L is independent of the angle α.

We have already seen that the orientation of the vector l in space is not random. The solution of the Schrödinger equation (Sect. 10.2) implies that when one axis is established, a component of the angular momentum is quantised. This axis can be

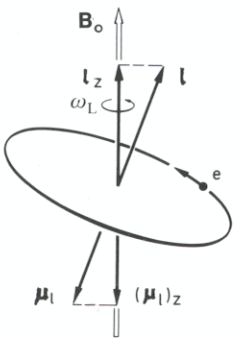

Fig. 12.6. Directional quantisation: Only the projections of the vectors l and μ_l on a chosen axis z can be observed. Here the z direction is the direction of B_0

determined by a magnetic field, for example. Therefore only discrete values of α, the angle between $\boldsymbol{B}$ and $\boldsymbol{l}$ or $\boldsymbol{\mu}_l$, are allowed.

According to Sect. 10.2, the following holds for the components of the angular momentum in the z direction:

$$l_z = m_l \hbar\,, \quad \text{with} \quad m_l = 0, \pm 1 \ldots \pm l\,. \tag{12.13}$$

Here m_l is used instead of m in Sect. 10.2. In this way we emphasise that $m(\equiv m_l)$ is associated with the *orbital* angular momentum. m_l is the *magnetic quantum number*. It can have $2l+1$ different values. Here l is again the angular momentum quantum number, $|\boldsymbol{l}| = \sqrt{l(l+1)}\,\hbar$. The largest possible component of $\boldsymbol{l}$ in the z direction thus has the value $l \cdot \hbar$.

The magnetic moment $\boldsymbol{\mu}_l$ associated with the orbital angular momentum is correspondingly quantised. For its component in the z direction the quantisation rule is

$$\mu_{l,z} = \frac{-e}{2m_0} l_z = -m_l \mu_\mathrm{B}\,. \tag{12.14}$$

The maximum value in the z direction is $l \cdot \mu_\mathrm{B}$. As a simplification (but not accurately), it is said that the state has the magnetic moment $l \cdot \mu_\mathrm{B}$.

Since $\boldsymbol{\mu}$ precesses around the direction of $\boldsymbol{B}$, it is intuitively clear that in an observation of the energy of interaction between the magnetic moment and the magnetic field, the x and y components of $\boldsymbol{\mu}$ are averaged out over time. However, the z component can be observed.

The experimental demonstration of the existence of a directional quantisation was provided by the Stern and Gerlach experiment (see Sect. 12.6).

12.4 Spin and Magnetic Moment of the Electron

The s states with orbital angular momentum $\boldsymbol{l} = 0$ have no orbital magnetic moment. Therefore, a one-electron atom should be diamagnetic in the ground state, when it has one valence electron in an outer shell and all the others in closed shells. However, these atoms are actually paramagnetic.

The reason is the existence of electron spin and the associated magnetic moment. Electron spin was introduced by *Uhlenbeck* and *Goudsmit* in 1925 to explain spectroscopic observations.

The splitting of many spectral lines in a magnetic field, which will be discussed later (the anomalous Zeeman effect) can only be explained if the electron has a spin angular momentum $\boldsymbol{s}$,

$$|\boldsymbol{s}| = \sqrt{s(s+1)}\,\hbar \tag{12.15}$$

and the associated magnetic moment

$$\boldsymbol{\mu}_\mathrm{s} = -g_\mathrm{s} \frac{e}{2m_0} \boldsymbol{s}\,, \tag{12.16}$$

where e is again the unit charge of the electron, without the negative sign. $s = 1/2$ is a new quantum number, the *spin quantum number*. The similarity of (12.16) and (12.10) is apparent. The two expressions differ only in that (12.16) contains the new factor g_s, the so-called g factor of the electron. Although the expected value for this proportionality constant on the basis of classical theory would be 1, the value has been empirically determined to be $g_s = 2.0023$. Figure 12.7 represents the spin and magnetic moment of the electron schematically.

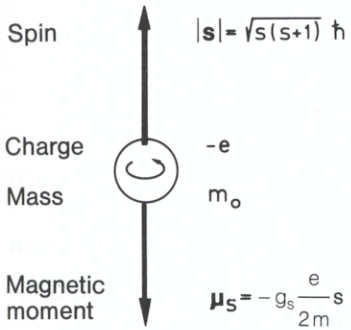

Fig. 12.7. Spin and magnetic moment of the electron

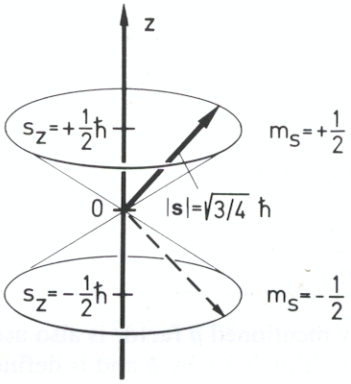

Fig. 12.8. The electron spin has two possible orientations in a magnetic field in the z direction. These are characterised by the quantum number $m_s = \pm 1/2$

Dirac showed in 1928 that the spin of the electron is a necessary consequence of a relativistic quantum theory (the Schrödinger theory is non-relativistic). The g factor $g_s = 2$ could also be thus derived. The slight difference between the predicted value of 2 and the empirical value can only be understood if the interaction of the electron with its own radiation field is taken into account through quantum electrodynamics.

As first shown by the experiment of *Stern* and *Gerlach* (Sect. 12.6), the spin can only have two orientations in an external magnetic field $\boldsymbol{B}$ (or in the presence of a defined z axis): "parallel" and "antiparallel" to the field (Fig. 12.8). Its components in this defined z direction are

$$s_z = m_s \hbar \quad \text{with} \quad m_s = \pm \tfrac{1}{2}; \tag{12.17}$$

m_s is the magnetic quantum number of the spin.

It follows from the orientation of the angular momentum that the magnetic moment is also oriented. The z component is

$$\mu_{s,z} = -g_s m_s \mu_B, \tag{12.18}$$

or numerically,

$$\mu_{s,z} = \pm 1.00116\, \mu_B. \tag{12.19}$$

Intuitively speaking, the spin and the magnetic moment precess around the field axis, leaving the z component constant (compare Sect. 12.3).

The gyromagnetic ratio, which was defined above (12.12) as the ratio between the magnetic moment and the angular momentum,

$$\gamma = \frac{|\mu|}{|l|} \quad \text{or} \quad \gamma = \frac{|\mu|}{|s|}, \tag{12.20}$$

is thus not the same for orbital (12.10) and spin (12.16) magnetism. For pure orbital magnetism,

$$\gamma_l = \frac{1}{2}\,\frac{e}{m_0},$$

and for pure spin magnetism,

$$\gamma_s = 1.00116\,\frac{e}{m_0}.$$

The previously mentioned g factor is also used instead of the gyromagnetic ratio γ. g is obtained by multiplying γ by $\hbar$ and is defined for pure orbital magnetism as

$$\gamma_l \hbar = \frac{1}{2}\,\frac{e}{m_0}\,\hbar = g_l \mu_B \tag{12.21}$$

and for pure spin magnetism by

$$\gamma_s \hbar = 1.00116\,\frac{e}{m_0}\,\hbar = g_s \mu_B = 2.0023\,\mu_B\,. \tag{12.22}$$

In the following, the reader will see that the easiest and most definitive way to calculate the magnetic properties of atoms is often to make use of measurements of the ratio γ or g.

12.5 Determination of the Gyromagnetic Ratio by the Einstein-de Haas Method

The gyromagnetic ratios of macroscopic samples can be measured as shown in Fig. 12.9. An iron needle is magnetised by a coil. If one changes the magnetisation of the sample – and this means changing the direction of the atomic magnetic moments in the sample – one will also change the direction of the atomic angular momenta, and this must be observable as a change in the angular momentum of the whole sample, according to the law of conservation of angular momentum. If the magnetisation is changed by 180° by reversing the poles of the coil, the angular momentum vector must also be rotated through 180°. Quantitatively, the change $\Delta\mu_N$ in the magnetisation of the needle, measured with a detection coil and a ballistic galvanometer, can be repre-

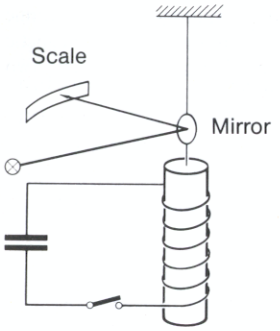

Fig. 12.9. *Einstein-de Haas* experiment. When the current in the coil is reversed, the magnetisable bar hanging in it turns. The torsion of the fibre on which the bar is suspended is measured with a mirror and light beam

sented as the sum of the changes for the individual electrons,

$$\sum_1^n \Delta\mu_z = n \cdot 2\mu_z ,$$

if n electrons have reversed their directions.

Likewise, the macroscopic change in the angular momentum of the needle, ΔL_N, measured by means of the torsion fibre, is the sum of the changes of the atomic angular momenta:

$$\sum_1^n \Delta l_z = n \cdot 2l_z .$$

For macroscopic samples, the measured ratio

$$\frac{\Delta\mu_N}{\Delta L_N} = \frac{\mu_z}{l_z} = \frac{e}{m_0} .$$

Thus according to the definition of (12.20),

$$\gamma = \frac{e}{m_0} \quad \text{or} \quad g = 2 .$$

From this experiment it can be seen that there is an angular momentum associated with the magnetism of atoms, and that it can be calculated as derived above.

In general, gyromagnetic ratio measurements, first described in 1915 by *Einstein* and *de Haas*, can indicate how much of the magnetism in a given sample is due to spin and how much to orbital angular momentum. However, a quantitative understanding of this type of measurement requires a deeper knowledge of solid state physics. There, it is found that in a solid, the orbital magnetic moment is often "quenched", i.e. it appears to be vanishingly small.

12.6 Detection of Directional Quantisation by Stern and Gerlach

In 1921, the deflection of atomic beams in inhomogeneous magnetic fields made possible

- the experimental demonstration of *directional quantisation* and
- the direct *measurement of the magnetic moments* of atoms.

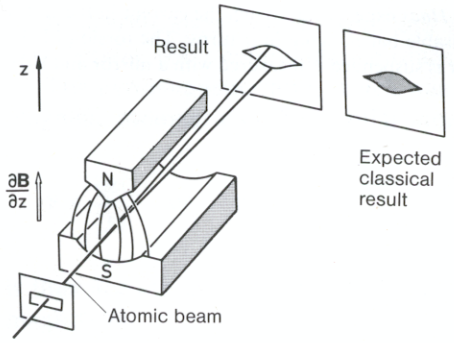

Fig. 12.10. *Stern-Gerlach* experiment. The atomic beam passes through an inhomogeneous magnetic field. One observes the splitting of the beam into two components

In the experiment (Fig. 12.10), one first generates a beam of atoms. In the first experiments of *Stern* and *Gerlach*, this was a beam of silver atoms which was generated in an atomic beam furnace and collimated by a series of slits. Later, hydrogen atoms from a gas discharge were also used. The collimated beam passes through a highly inhomogeneous magnetic field, with the direction of the beam perpendicular to the direction of the field and of the gradient. The directions of the field and gradient are the same. Without the field, the vectors of the magnetic moments and angular momenta of the atoms are randomly oriented in space. In a homogeneous field, these vectors precess around the field direction z.

An inhomogeneous field exerts an additional force on the magnetic moments. The direction and magnitude of this force depends on the relative orientation between the magnetic field and the magnetic dipole. A magnetic dipole which is oriented parallel to the magnetic field moves in the direction of increasing field strength, while an antiparallel dipole moves towards lower field strength. A dipole which is perpendicular to the field does not move.

The deflecting force can be derived from the potential energy in the magnetic field $V_{\text{mag}} = -\boldsymbol{\mu} \cdot \boldsymbol{B}$:

$$F_z = \mu_z \frac{dB}{dz} = \mu \frac{dB}{dz} \cos\alpha\,, \tag{12.23}$$

where α is the angle between the magnetic moment and the direction of the field gradient.

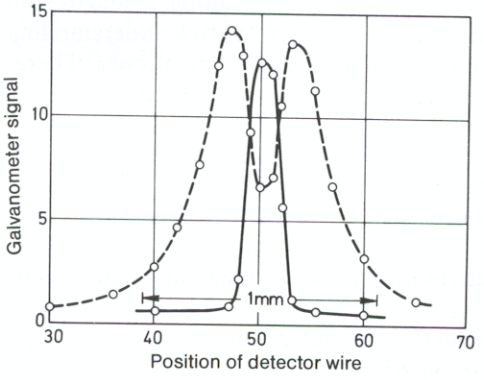

Fig. 12.11. *Stern-Gerlach* experiment. Observed intensity distribution of an atomic beam with and without an applied magnetic field, $^2S_{1/2}$ state [from H. Kopfermann: *Kernmomente*, 2nd ed. (Akademische Verlagsgesellschaft, Frankfurt 1956)]

In classical mechanics, any orientation α of the atomic magnet with respect to the field is allowed. Atoms with magnetic moments perpendicular to the field gradient are not deflected. Those in which the vectors are parallel are deflected the most, and all possible intermediate values can occur. In the classical picture one thus expects a continuum of possible deflections. With H and Ag atoms, however, two rather sharp peaks separated by 2δ were observed on the detector (Fig. 12.11).

This experiment and similar measurements on other atoms permit the following conclusions:

- There is a *directional quantisation.* There are only discrete possibilities for the orientation relative to a field $\boldsymbol{B}_0$, in this case two, parallel and antiparallel.
- From a quantitative evaluation of the observed deflection δ in the above example, one obtains the value $\mu_z = \pm\mu_B$. In general this method provides observed values for *atomic magnetic moments* if the magnitude of the field gradient is known.
- For all atoms which have an s electron in the outermost position, one obtains the same value for the deflecting force, from which it follows that the *angular momenta and magnetic moments of all inner electrons cancel each other* and one measures only the effect of the outermost s electron.
- The s electron has an *orbital angular momentum* $l = 0$ and one observes only spin magnetism.
- Like gyroscopes, atoms maintain the magnitude and direction of their angular momenta in the course of their motion in space.

This experiment provides the basis for the knowledge of the angular momenta and magnetic moments of atoms which was summarised in Sects. 12.2 and 12.3.

12.7 Fine Structure and Spin-Orbit Coupling: Overview

In the introductory section to this chapter we mentioned that all energy terms – with the exception of the s states of one-electron atoms – are split into two substates. This produces a doublet or multiplet structure of the spectral lines, which is denoted by the generic name *fine structure.*

The fine structure cannot be explained with the Coulomb interaction between the nucleus and the electrons. Instead, it results from a magnetic interaction between the orbital magnetic moment and the intrinsic moment of the electron, the *spin-orbit coupling.* Depending on whether the two moments are parallel or antiparallel, the energy term is shifted somewhat.

The magnetic coupling energy between the orbital moment and the spin moment will be calculated in Sect. 12.8. The coupling of the magnetic moments leads to an addition of the two angular momenta to yield a total angular momentum.

The following conclusions are then valid (Fig. 12.12):

- $\boldsymbol{l}$ and $\boldsymbol{s}$ add to give a total angular momentum $\boldsymbol{j}$;
- $\boldsymbol{j}$ has the magnitude $\sqrt{j(j+1)}\,\hbar$ with $j = |l \pm s|$, i.e. $j = |l \pm \frac{1}{2}|$ for the case treated here of a single-electron system with $s = \frac{1}{2}$. The quantum number j is a new quantity: the quantum number of the total angular momentum. We shall show with a quantum mechanical calculation in Sect. 14.3 that $\boldsymbol{j}$ has the magnitude given above.
- For a p electron with $l = 1$, $s = \frac{1}{2}$, we find the following possibilities:

$$j = 3/2\,, \quad |\boldsymbol{j}| = \sqrt{15/2}\,\hbar\,, \quad \text{and}$$
$$j = 1/2\,, \quad |\boldsymbol{j}| = \sqrt{3/2}\,\hbar\,;$$

- when $l = 0$, $j = s$ and there is no doublet splitting;
- for $\boldsymbol{j}$, just as for $\boldsymbol{l}$, there is a directional quantisation. The z components must obey the condition

$$j_z = m_j \hbar\,, \quad m_j = j, j-1, \ldots -j \quad (2j+1 \text{ possibilities})\,.$$

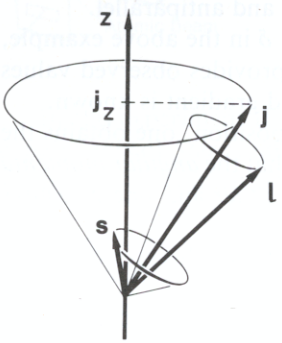

Fig. 12.12. Coupling of the vectors of spin s and orbital angular momentum l to give the total (resultant) angular momentum j in the vector model. The vectors s and l precess about the resultant j. In a magnetic field applied in the z direction, j precesses about z. The opening angle of the cone of precession is determined by the magnetic quantum number m_j. The figure shows the case $s = 1/2$, $l = 2$, $j = 5/2$

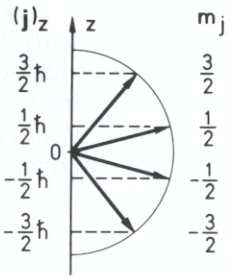

Fig. 12.13. Directional quantisation: for the z component of the angular momentum j, only certain discrete values are allowed. They are denoted by the magnetic quantum number m_j. For the case illustrated, $j = 3/2$, the magnitude of the vector is $|\boldsymbol{j}| = \sqrt{(3/2)(5/2)}\,\hbar$. Four orientations are allowed: $m_j = 3/2,\ 1/2,\ -1/2,\ -3/2$

For example, a state with $j = 3/2$ is fourfold degenerate (Fig. 12.13).

- A magnetic moment $\boldsymbol{\mu}_j$ is associated with j; this will be calculated in Sect. 13.3.5.
- For optical transitions, a selection rule $\Delta j = 0$ or ± 1 is valid; however, a transition from $j = 0$ to $j = 0$ is always forbidden. This selection rule may be considered to be an empirical result, derived from the observed spectra. The reasons for it will become clear later (Chap. 16).

12.8 Calculation of Spin-Orbit Splitting in the Bohr Model

In this section, we shall calculate the energy difference between the parallel and the antiparallel orientations of the orbital angular momentum and the spin. For this purpose, the simple Bohr model will be used as starting point; the quantum mechanical treatment will be discussed in Sect. 14.3.

The motion of the electron around the nucleus generates a magnetic field $\boldsymbol{B}_l$ at the site of the electron. This field interacts with the magnetic moment of the electron. To determine the magnitude of this magnetic field, we borrow from relativity theory and assume that the electron is stationary and that the nucleus moves instead (Fig. 12.14). We replace the position vector for the orbiting electron, $\boldsymbol{r}$, by the vector $-\boldsymbol{r}$.

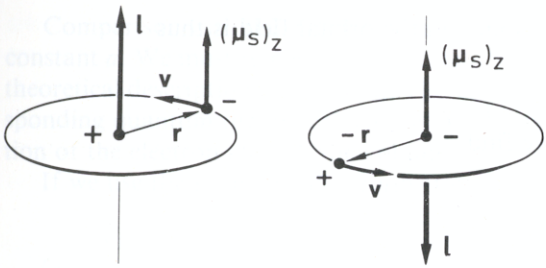

Fig. 12.14. For the calculation of spin-orbit coupling, the system with the nucleus at rest (*left*) is transformed to the system with the electron at rest (*right*). The vector r is replaced by the reversed vector $-r$

The magnetic field of the moving charge $+Ze$ is found from the Biot-Savart law to be

$$\boldsymbol{B}_l = +\frac{Ze\mu_0}{4\pi r^3}[v \times (-r)] \tag{12.24}$$

or

$$\boldsymbol{B}_l = -\frac{Ze\mu_0}{4\pi r^3}[v \times r]\,. \tag{12.25}$$

Angular momentum is defined as $\boldsymbol{l} = r \times m_0 v$ or $-\boldsymbol{l} = m_0 v \times r$. Then

$$\boldsymbol{B}_l = \frac{Ze\mu_0}{4\pi r^3 m_0}\boldsymbol{l}\,, \tag{12.26}$$

where m_0 is the rest mass of the electron.

The magnetic field which is generated by the relative motion of the nucleus and the electron is thus proportional and parallel to the orbital angular momentum of the electron. We still require the back transformation to the centre-of-mass system of the atom, in which the nucleus is essentially at rest and the electron orbits around it. A factor 1/2 occurs in this back transformation, the so-called Thomas factor, which can only be justified by a complete relativistic calculation. The particle in its orbit is accelerated, and from the viewpoint of the proton, the rest system of the electron rotates one additional time about its axis during each revolution around the orbit. The back transformation is therefore complicated and will not be calculated in detail here.

The magnetic moment of the electron, and with it, its coupled spin vector, precess about the magnetic field $\boldsymbol{B}_l$ produced by the orbital motion (cf. Fig. 12.15).

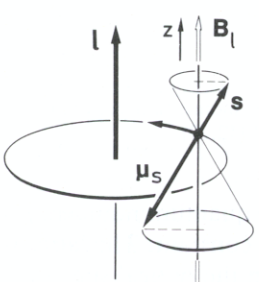

Fig. 12.15. Precession of the spin about the magnetic field $\boldsymbol{B}_l$ associated with the orbital angular momentum, with the components s_z and $\mu_{s,z}$

The interaction energy between the spin and the orbital field is thus

$$V_{l,s} = -\boldsymbol{\mu}_s \cdot \boldsymbol{B}_l .$$

Substituting – see (12.16), $g_s = 2$ – we find

$$V_{l,s} = 2\frac{e}{2m_0}(\boldsymbol{s} \cdot \boldsymbol{B}_l) ,$$

and with (12.26)

$$= \frac{Ze^2\mu_0}{8\pi m_0^2 r^3}(\boldsymbol{s} \cdot \boldsymbol{l}) . \tag{12.27}$$

Here we have included the (underived) Thomas correction; this gives the factor 8 in the denominator (instead of 4).

In order to get a feeling for the order of magnitude, we set $Z = 1$ and $r = 1$ Å and obtain $V_{l,s} \cong 10^{-4}$ eV. The field produced by the orbital motion at the position of the electron is found to be about 1 tesla $= 10^4$ gauss. The fields associated with the orbital angular momentum are thus – for small values of Z – of the same order of magnitude as may be readily produced in the laboratory.

Equation (12.27) may also be written in the form

$$V_{l,s} = \frac{a}{\hbar^2}\boldsymbol{l} \cdot \boldsymbol{s} = \frac{a}{\hbar^2}|\boldsymbol{l}||\boldsymbol{s}|\cos(\boldsymbol{l},\boldsymbol{s}) \tag{12.28}$$

where $a = Ze^2\mu_0\hbar^2/(8\pi m_0^2 r^3)$. The scalar product $\boldsymbol{l} \cdot \boldsymbol{s}$ may be expressed in terms of the vectors $\boldsymbol{l}$ and $\boldsymbol{s}$ by using the law of cosines according to Fig. 12.16, where we recall that $\boldsymbol{l}^2$ must be replaced by its quantum value $l(l+1)\hbar^2$, etc. We thus obtain for the spin-orbit coupling energy

$$V_{l,s} = \frac{a}{2\hbar^2}(|\boldsymbol{l}+\boldsymbol{s}|^2 - |\boldsymbol{l}|^2 - |\boldsymbol{s}|^2)$$

$$= \frac{a}{2\hbar^2}(|\boldsymbol{j}|^2 - |\boldsymbol{l}|^2 - |\boldsymbol{s}|^2)$$

$$= \frac{a}{2}[j(j+1) - l(l+1) - s(s+1)] . \tag{12.29}$$

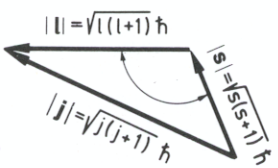

Fig. 12.16. Vector addition of the angular momentum vectors to the total angular momentum $\boldsymbol{j}$, explanation of (12.29)

The spin-orbit coupling energy is thus expressed in terms of the quantum numbers j, l and s, as well as a constant a, known as the spin-orbit coupling constant. The latter is directly measurable by determination of the doublet structure in the optical spectra.

Comparison with (12.27) shows that the orbital radius r is included in this coupling constant a. We must remember, however, that there are no fixed orbits in the quantum theoretical description of the atom. Therefore it is necessary to replace r^{-3} by the corresponding quantum theoretical average $\overline{1/r^3} = \int(|\psi|^2/r^3)\,dV$, where ψ is the wavefunction of the electron and dV the volume.

If we use the radius r_n of the nth Bohr radius as a rough approximation for r,

$$r_n = \frac{4\pi\varepsilon_0\hbar^2 n^2}{Ze^2 m_0}\,, \tag{12.30}$$

we obtain

$$a \sim \frac{Z^4}{n^6}\,.$$

If instead we use the above-defined average value $\overline{r^{-3}}$, we obtain for atoms similar to H

$$a \sim \frac{Z^4}{n^3 l(l+\frac{1}{2})(l+1)}\,, \tag{12.31}$$

which will not be derived here.

Let us again summarise what we know about the fine structure of one-electron states:

- Interaction of the electron with the orbital angular momentum or the orbital moment splits each level into two. The result is doublet levels; for example in the upper state of the sodium D lines, the $3P$ state is split into the $3P_{1/2}$ and the $3P_{3/2}$ states (Fig. 12.17).

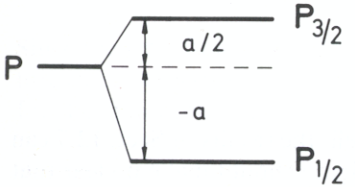

Fig. 12.17. Fine structure splitting of the P state in the one electron system into the two states $P_{3/2}$ and $P_{1/2}$. The magnitude of the splitting is given by (12.29). Since only one electron is involved, one can also use lower case "p"

- For s terms there is no splitting, because there is no magnetic field with which the spin can align itself.
- Levels with higher values of the quantum number j have higher energies (12.29).
- The fine structure splitting $V_{l,s}$ is proportional to the fourth power of the nuclear charge.

The fine structure is therefore difficult to observe in the H atom. For the H_α, H_β, and H_γ lines of the Balmer series (6562.79, 4861.33 and 4340.46 Å), the splitting is 0.14, 0.08 and 0.07 Å, respectively. This corresponds to a wavenumber of 0.33 cm^{-1} for the H_α line, which is in the microwave range – if one wished to observe it directly. A direct observation of the splitting of optical spectral lines into two very close components is not possible by conventional spectroscopy because of Doppler broadening of the lines. In the lithium atom, the splitting of the first resonance line

is likewise only 0.337 cm^{-1}. By contrast, the observed values for a line pair of the 1st primary series, i.e. for the first resonance lines, of cesium ($Z = 55$, $n = 6$) are $\lambda = 8943$ Å and 8521 Å. The splitting is thus $\Delta\lambda = 422$ Å or $\Delta\bar{\nu} = 554\ cm^{-1}$. It is so large, in fact, that the two lines are difficult to recognise as components of a pair. The sodium atom ($Z = 11$, $n = 3$) lies between these extremes: the yellow D lines D_1 and D_2 are separated by $\Delta\lambda = 6$ Å, which corresponds to 17.2 cm^{-1}.

– The splitting is greatest for the smallest principal quantum number n (12.31).

We can now expand upon the symbolism needed to identify the energy terms of atoms. The terms for orbital angular momentum are generally indicated by upper case letters S, P, D, F, etc. The principal quantum number n is written as an integer in front of the letter, and the total angular momentum quantum number j as a subscript. The multiplicity $2s+1$ is indicated by a superscript to the left of the orbital angular momentum letter. For single-electron systems, the terms are doublet terms, because the spin of the single electron can have two orientations with respect to the orbital angular momentum.

The S terms are not split. Nevertheless, one writes the multiplicity 2 even for S terms in one-electron systems.

One thus has the following symbols:

$2^2S_{1/2}$ for a state in which the valence electron has the quantum numbers $n = 2$, $l = 0$, $j = 1/2$.

$2^2P_{1/2}$, $2^2P_{3/2}$ for states in which the valence electron has the quantum numbers $n = 2$, $l = 1$, $j = 1/2$ or $3/2$, respectively.

In general, the symbolism is $n^{2S+1}L_J$. The upper case letters S (spin quantum number), L (orbital angular momentum quantum number) and J (total angular momentum quantum number) apply to several-electron atoms, while the corresponding lower case letters apply to single electrons.

12.9 Level Scheme of the Alkali Atoms

For an atom with one electron in the incomplete outer shell, the results of Sect. 12.7 can be summarised in the term scheme of Fig. 12.18. This figure should make it clear that both the lifting of orbital degeneracy (i.e. the energy difference between terms with the

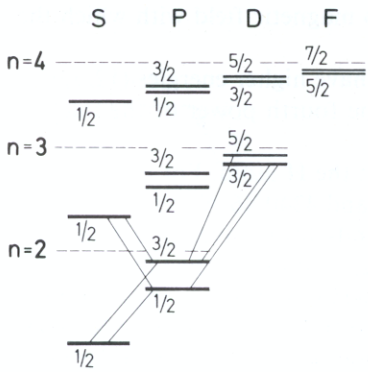

Fig. 12.18. Term scheme for alkali atoms, i.e. one-electron states, including the spin-orbit splitting. The levels are not shown to scale. A few allowed transitions are indicated. The terms are displaced with respect to those of the H atom ($n = 2, 3, 4$, *left side*, *dashed lines*), the s terms most. The fine structure splitting decreases with increasing values of n and l

same n but different l quantum numbers) and spin-orbit splitting become smaller as the quantum numbers n and l increase.

The optical transitions in the term scheme obey the rules $\Delta l = \pm 1$, $\Delta j = \pm 1$ or 0. Optical transitions are thus allowed only if the angular momentum changes. The total angular momentum j, however, can remain the same. This would happen if the orbital angular momentum and the spin changed in opposite directions.

The first principal series of the alkali atom arises from transitions between the lowest $^2S_{1/2}$ term (i.e. $n = 2, 3, 4, 5, 6$ for Li, Na, K, Rb, Cs) and the P terms $^2P_{1/2}$ and $^2P_{3/2}$. Since the S terms are single-valued, one sees pairs of lines. The same holds for the sharp secondary series, which consists of transitions between the two lowest P terms $n^2P_{3/2}$ ($n = 2, 3, 4, 5, 6$ for Li, Na, K, Rb, Cs) and all higher $^2S_{1/2}$ terms. The lines of the diffuse secondary series, however, are triple (Fig. 12.19), because both the P and the D terms are double.

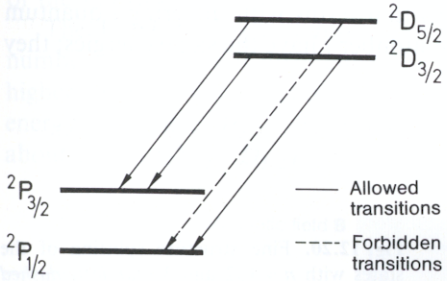

Fig. 12.19. Allowed and forbidden transitions between P and D states of the alkali atom, here for a triplet of the diffuse secondary series. This is a section from Fig. 12.18

12.10 Fine Structure in the Hydrogen Atom

Since the wavefunctions of the H atom are known explicitly (Chap. 10), its fine structure can be exactly calculated. The starting point is the expression derived above (12.27) for the spin-orbit splitting energy:

$$V_{l,s} = \frac{e^2 \mu_0}{8 \pi m_0^2} \cdot \frac{1}{r^3} (s \cdot l) \,. \tag{12.32}$$

We use the solution of the non-relativistic Schrödinger equation for the H atom, which provides the energy states $E_{n,l}$ (Sect. 10.4). For the H atom, both the relativity correction (cf. Sect. 8.10) and the fine structure interaction are small compared to the energies $E_{n,l}$, but the two are of comparable magnitude. One can therefore calculate the two corrections separately and write

$$E_{n,l,j} = E_{n,l} + E_{\text{rel}} + E_{l,s} \,.$$

The two correction terms, the one for the relativistic mass change E_{rel} and the other for the spin-orbit coupling $E_{l,s}$, together give the fine structure correction E_{FS}. These terms will not be calculated in detail here. The complete calculation was carried out by *Dirac*.

As a result, one obtains

$$E_{FS} = -\frac{E_n \alpha^2}{n}\left(\frac{1}{j+1/2} - \frac{3}{4n}\right)\cdot Z^2 \,, \tag{12.33}$$

where

$$\alpha = \frac{e^2}{4\pi\varepsilon_0 \hbar c}\left(\text{or } \frac{\mu_0 c}{4\pi\hbar} e^2\right),$$

which is the Sommerfeld fine structure constant which was introduced in Sect. 8.10.

By including the spin-orbit coupling, one thus obtains the same result as earlier (Sect. 8.10) in the calculation of the relativistic correction, the only change being that l has been replaced by j. The energy shift with respect to the previously calculated energy terms $E_{n,l}$ is of the order of α^2, i.e. $(1/137)^2$, and is thus difficult to measure.

The most important result of (12.33) is the fact that the fine structure energy of the H atom depends only on j, not on l. This means that terms with differing l quantum numbers (for the same n) and the same quantum number j have the same energies; they are energetically degenerate (Fig. 12.20).

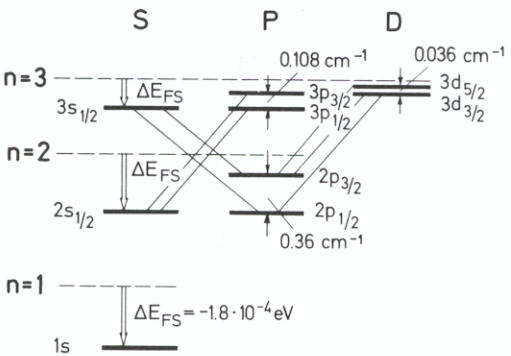

Fig. 12.20. Fine structure splitting of the states with $n = 1, 2$ and 3 (*far left, dashed lines*, the levels without fine structure), according to *Dirac* (not to scale). The fine structure shifts are indicated by open arrows. States with the same l are degenerate without fine structure interactions. States with the same j have the same energy if fine structure is taken into account

The fine structure of the hydrogen lines is thus quantitatively accounted for. The fine structure energies of heavier atoms are larger and are thus easier to observe. Their calculations, however, are far more difficult, because the exact calculation of the wavefunctions of atoms with more than one electron is far more complex.

12.11 The Lamb Shift

In the years 1947 – 1952, *Lamb* and *Retherford* showed that even the relativistic Dirac theory did not completely describe the H atom. They used the methods of high-frequency and microwave spectroscopy to observe very small energy shifts and splitting in the spectrum of atomic hydrogen. In other words, they used the absorption by H atoms of electromagnetic radiation from high-frequency transmitters or klystron tubes. They could, in this way, observe energy differences between terms with the same j, namely differences of 0.03 cm^{-1} – this corresponds to a difference of 900 MHz – between the terms $2^2S_{1/2}$ and $2^2P_{1/2}$.

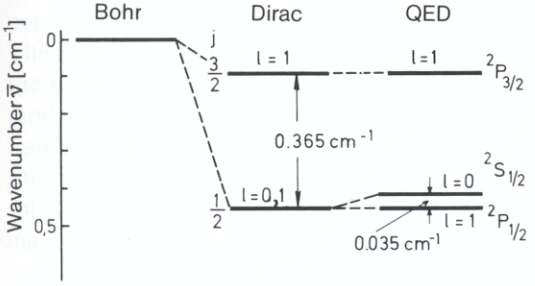

Fig. 12.21. The Lamb shift: fine structure of the $n = 2$ level in the H atom according to *Bohr*, *Dirac* and quantum electrodynamics taking into account the Lamb shift. The j degeneracy is lifted

They achieved a precision of 0.2 MHz. Figure 12.21 shows the corresponding energy diagram.

Like the fine structure, this small energy shift was not observable by means of optical spectroscopy as a splitting of the H_α line of hydrogen, because the Doppler broadening of the spectral lines due to the motion of the atoms exceeded the magnitude of the splitting.

The Lamb-Retherford result can be generalised: levels with the same quantum numbers n and j, but different l, are not exactly the same. Rather, all $S_{1/2}$ terms are higher than the corresponding $P_{1/2}$ terms by an amount equal to about 10% of the energy difference $(P_{3/2} - P_{1/2})$, and the $P_{3/2}$ terms are higher than the $D_{3/2}$ terms by about 2‰ of $(D_{5/2} - D_{3/2})$.

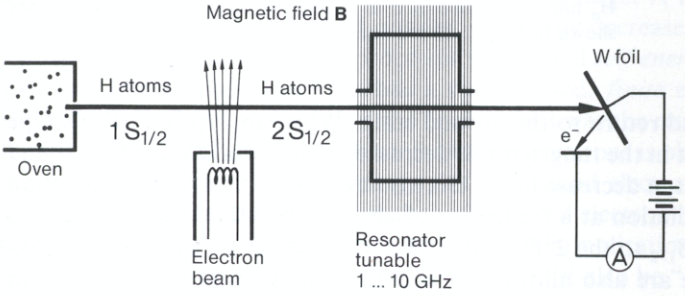

Fig. 12.22. Arrangement for measurement of the Lamb shift. A beam of H atoms is excited to the metastable $2S_{1/2}$ state by bombardment with electrons. The beam passes through a resonator. If electromagnetic transitions are induced there, the number of excited atoms reaching the tungsten foil receiver is lower, and the measured electron current correspondingly drops. The magnetic field $\boldsymbol{B}$ serves to create an additional energetic separation between the $S_{1/2}$ and the $P_{1/2}$ states. This prevents mixing of those states and thereby avoids an immediate decay via the $2P_{1/2}$ state

The Lamb and Retherford experiment is shown in Fig. 12.22. A beam of hydrogen atoms is generated from H_2 molecules by thermal dissociation at 2500°C. A small number of these atoms is excited to the metastable state $2^2S_{1/2}$ by bombardment by electrons. Optical transitions between this state and the ground state $1^2S_{1/2}$ are forbidden. The atoms then pass through a tunable resonator for high-frequency or microwave radiation, to a tungsten foil. There the metastable atoms can give up their excitation energy, thereby releasing electrons from the surface of the metal. The electron current is measured and serves as an indicator of the rate at which atoms in the $2^2S_{1/2}$ state arrive at the detector. Those atoms which are excited to the $2^2P_{3/2}$ state by absorbing microwaves in the range of 10000 MHz in the resonator (compare term scheme in Fig. 12.21) can emit light at the wavelength of the H_α line (or more exactly, of one

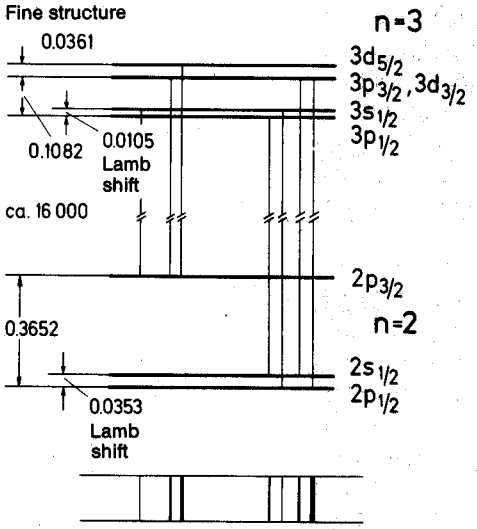

Fig. 12.23. Structure of the H_α line of hydrogen and term scheme including the fine structure. The expected optical spectrum is shown below (ignoring the line widths). Darker lines indicate higher intensity. The wavenumbers are in cm^{-1}

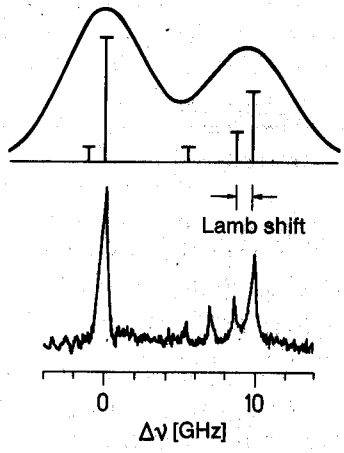

Fig. 12.24. *Above:* Structure of H_α line of the hydrogen atom at room temperature. The linewidth and thus the spectral resolution is determined by the Doppler width. *Below:* The method of Doppler-free spectroscopy (saturated absorption using a dye laser, Sect. 22.3) allows resolution of the individual components of the H_α line (after *Hänsch* et al.). The two additional very weak lines shown in Fig. 12.23 are omitted in Fig. 12.24

component of this line) and return to the ground state. When absorption of this type occurs, the electron current in the tungsten foil decreases. *Lamb* and *Retherford* found in 1947 that the same effect, a decrease in the electron current, occurred on absorption or induced emission of radiation at a frequency of about 1000 MHz. This was due to the transition from the $2^2S_{1/2}$ to the $2^2P_{1/2}$ state. From the latter state, radiative transitions to the ground state are also allowed. It was thus shown that even states with the same total angular momentum j are energetically different.

The term scheme of an atom can be refined for optical transitions as well. Figure 12.23 shows the complete term scheme for the H_α line of the hydrogen atom. This line

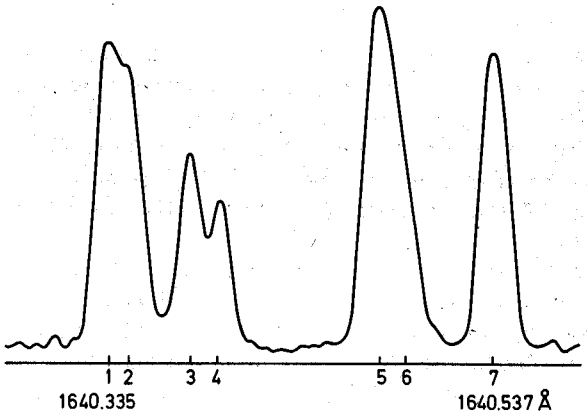

Fig. 12.25. Lamb shift and fine structure of the helium atom: fine structure at 1640 Å. Seven components are observed. The lines 1, 2 and 3, 4 would be unsplit without the Lamb shift. [From G. Herzberg: Trans. Roy. Soc. Can. **5**, (1967) Fig. 5]

consists of 7 components of different intensities in an energy range of about 0.4 cm^{-1}. The upper part of Fig. 12.24 shows the structure of the H_α line, as it can be observed in the presence of Doppler broadening. The lower part shows a curve obtained by the modern method of Doppler-free spectroscopy (Sect. 22.3). With this method, the Lamb shift can also be seen in optical spectra. The fine structure splitting and the Lamb shift are larger in the heavier helium atom, so that direct optical observation of the splitting is easier than with the H atom. Even without removing the Doppler broadening, the fine structure can be resolved, as Fig. 12.25 shows.

The Lamb shift was of utmost importance for the development of quantum electrodynamics. Previously, this theory treated only the emission and absorption of light quanta in atomic transitions. To explain the Lamb shift, it was necessary to go one step further. It had to be assumed that the electrons in an atom were continually emitting and reabsorbing light quanta, in which process energy conservation can apparently be violated.

This "violation of energy conservation" must not, to be sure, be taken too literally. According to the uncertainty relation between energy and time (7.29), the energy is only sharply defined when a measurement is performed over a sufficiently long period of time. It is thus completely consistent with energy conservation that an electron can emit a quantum even without having the necessary energy, as long as the quantum is reabsorbed quickly enough. Much more decisive for the theoreticians was, however, the recognition that the energy shifts in the atomic levels (on a negative energy scale) produced by these "virtual" processes were infinitely large. A free electron can also continually emit and absorb virtual quanta; its energy decreases infinitely in the process. Energy shifts caused by virtual processes are termed *self energy*. Experimentally, a free electron, like a bound electron, has a well-defined, *finite* energy. The basic idea for solving the "infinity problem" of the energy shift was the recognition that only the difference between the energies of bound and free electrons is physically interesting. Or, in other words: to calculate the energy shift of bound electrons, one must subtract the self-energy of a free electron from that of a bound electron in a particular atomic state (cum grano salis). This process is termed "renormalisation". Since the masses also become infinite due to virtual processes, they must also be "renormalised". Naturally, at first glance it seems very adventurous to subtract two infinite quantities from one another in order to obtain a well-defined finite result. In the framework of quantum electrodynamics, however, it was found possible to set up well-defined rules for the renormalisation procedure, and the Lamb shift can be calculated today with great precision. The important result is that the validity of quantum electrodynamics can therefore be tested – and has been verified – in an excellent manner.

A summary of the theoretical treatment is given in Sect. 15.5.2. In preparation for this treatment, in Sect. 15.5.1 we introduce the quantisation of the electromagnetic field, which follows immediately from the quantisation of the harmonic oscillator. As is shown in one of the problems for Sect. 15.5.1, the theory of the Lamb shift has a surprisingly simple physical explanation: the quantum-mechanical zero-point fluctuations of the electromagnetic field act statistically on the electrons and thus cause a shift of their potential energy.

Problems

12.1 Calculate the precessional frequency of electrons and of protons [$I = 1/2$, magnetic moment $= (2.79/1836)\cdot\mu_B$] in the magnetic field of the earth ($\simeq 2\cdot 10^{-5}$ tesla).

12.2 In the Stern-Gerlach experiment, a beam of silver atoms in the ground state ($5^2S_{1/2}$) is directed perpendicularly to a strong inhomogeneous magnetic field. The field gradient is $dB/dz = 10^3$ tesla/m. In the direction of the atomic beam, the magnetic field extends a distance of $l_1 = 4$ cm, and the catcher screen is a distance $l_2 = 10$ cm from the magnet. Calculate the components of the magnetic moment in the direction of the magnetic field, if the splitting of the beam at the screen is observed to be $d = 2$ mm, and the velocity of the atoms is $v = 500$ m/s. The average mass of silver atoms is $M = 1.79 \cdot 10^{-25}$ kg. Why doesn't the nuclear spin affect the experiment?

12.3 How large is the magnetic field generated by the electron in the ground state of a hydrogen atom, at the position of the proton if it would circulate according to Bohrs model on the shell $n = 1$?

12.4 How large is the magnetic moment of the orbital motion in a muonium atom, in which the electron of a ground-state hydrogen atom has been replaced by a muon? How large is the moment in positronium (an electron and a positron, i.e. particles with the mass of the electron and opposite charges, moving around the common centre of mass)?

12.5 Calculate the spin-orbit splitting of the states of the hydrogen atom with $n = 2$ and $n = 3$ using the relations

$$V_{l,s} = \frac{1}{\pi}\frac{Ze^2\mu_0}{8\pi m_0^2 r^3}(s\cdot l) \ ,$$

and

$$r^{-3} = \frac{Z^3}{a_0^3 n^3 l(l+\frac{1}{2})(l+1)} \ .$$

What are the values for a Rydberg state with $n = 30$ for the largest ($l = 1$) and the smallest ($l = 29$) splitting?
a_0 is the radius of the innermost Bohr orbit.

12.6 In the cesium atom, spin-orbit splitting between the states $6P_{1/2}$ and $6P_{3/2}$ leads to a wavelength difference of $\Delta\lambda = 422$ Å for the first line pair of the primary series, with $\lambda = 8521$ Å for the line with the shorter wavelength. Calculate from this the fine structure constant a and the field at the nucleus B_1. Use (12.27).

12.7 Sketch the energy levels of the hydrogen atom, including the fine structure, up to $n = 3$. Show the possible transitions. How many different lines are there?

12.8 The fine structure in hydrogen-like ions (ions with only one electron) is described by (12.33).

a) Show that the correction term does not disappear for any possible combination of the quantum numbers n and j, but that it always reduces the value of the uncorrected energy.
b) Into how many energy levels are the terms of singly charged helium with the principal quantum numbers $n = 3$ and $n = 4$ split by the fine structure interaction?
c) Sketch the positions of these levels relative to the non-shifted terms and give the amount of the shift.
d) Determine which transitions are allowed, using the selection rules $\Delta l = \pm 1$, $\Delta j = 0$ or ± 1.

12.9 Give the relative splitting of the various levels of an LSJ multiplet due to spin-orbit interaction for the ${}^3F$ and ${}^3D$ multiplets. Sketch the energy levels of these multiplets and indicate with arrows the allowed ${}^3F \rightarrow {}^3D$ transitions. Repeat the above process for the ${}^4D \rightarrow {}^4P$ and ${}^4P \rightarrow {}^4S$ transitions.

12.10 The interaction energy E between two magnetic moments μ_1 and μ_2 is (r = the radius vector of μ_1 and μ_2):

$$E = +\frac{\mu_0}{4\pi}\left\{\frac{\mu_1 \cdot \mu_2}{r^3} - 3\frac{(\mu_1 \cdot r)(\mu_2 \cdot r)}{r^5}\right\}.$$

a) Under which conditions is $E = 0$ for a given $|r|$?
b) For parallel moments, which arrangement yields an extreme value for E?
c) For case b) with $|r| = 2$ Å, calculate the energy for the electron-electron and proton-proton interactions. In each case, how large is the magnetic field at μ_2 due to μ_1 ($\mu_{\text{proton}} = 1.4 \cdot 10^{-26}$ A m^2)?

13. Atoms in a Magnetic Field: Experiments and Their Semiclassical Description

13.1 Directional Quantisation in a Magnetic Field

In the previous chapters, we have already seen that a directional quantisation exists. The angular momentum vectors in an atom can only orient themselves in certain discrete directions relative to a particular axis (the quantisation axis). The directional quantisation is described by the magnetic quantum number m. In an applied magnetic field $\boldsymbol{B}_0$, the interaction energy between the field and the magnetic moment of the electrons in an atom, which we have already calculated, leads to a splitting of the energy terms, which is described by the different possible values of the magnetic quantum number. We shall concern ourselves in this chapter with the measurement of this energy splitting.

A first application of the splitting of atomic states in a magnetic field to the determination of the magnetic moments of the atoms was already discussed in the treatment of the Stern-Gerlach experiment. In the following, we shall consider some other types of experiments.

13.2 Electron Spin Resonance

The method of electron spin resonance (abbreviated ESR, sometimes EPR for electron paramagnetic resonance) involves the production of transitions between energy states of the electrons which are characterised by different values of the magnetic quantum number m. In general, the degeneracy is lifted by the application of an external magnetic field; the transition frequencies, which are usually in the range of microwave frequencies, depend on the strength of the applied field. With this technique, one can observe transitions between states of different magnetic quantum number directly. In Zeeman spectroscopy, to be described later, the transitions observed are in the optical region, and their response to magnetic fields is studied; in this case, the transitions cause changes in not only the magnetic quantum number, but also in the other quantum numbers.

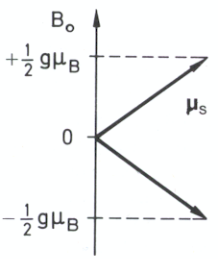

Fig. 13.1. The spin of an electron, and thus its magnetic moment, have two possible orientations in an applied magnetic field. They correspond to two values of the potential energy

The principle of ESR may be easily understood by considering the magnetic moment produced by the spin of a free electron in a magnetic field $\boldsymbol{B}_0$ (Fig. 13.1).

An electron has the magnetic moment

$$\mu_s = \sqrt{s(s+1)}\,\mu_B g_s \tag{13.1}$$

with the possible components along the quantisation axis z of the field $\boldsymbol{B}_0$

$$(\mu_s)_z = \pm \tfrac{1}{2} g_s \mu_B \,. \tag{13.2}$$

The potential energy of these two orientations differs by the amount

$$\Delta E = g_s \mu_B B_0 \,. \tag{13.3}$$

If a sinusoidally varying magnetic field $\boldsymbol{B}_1 = \tilde{\boldsymbol{B}}_1 \sin \omega t$ is now applied in a direction perpendicular to $\boldsymbol{B}_0$, transitions between the two states are induced if the frequency $\nu = \omega/2\pi$ fulfils the condition

$$\Delta E = h\nu = g_s \mu_B B_0 \,, \tag{13.4}$$

or, in numbers,

$$\nu = 2.8026 \cdot 10^{10} \cdot \boldsymbol{B}_0 \,\mathrm{Hz\,(tesla)^{-1}} \,. \tag{13.5}$$

The transitions with $\Delta m = \pm 1$ are allowed magnetic dipole transitions. A quantum mechanical treatment of ESR will follow in Chap. 14. The frequency which must be used depends, according to (13.5), on the choice of the applied magnetic field $\boldsymbol{B}_0$. For reasons of sensitivity, usually the highest possible frequencies are used, corresponding to the highest possible magnetic fields. The fields and frequencies used in practice are, of course, limited by questions of technical feasibility; usually, fields in the range 0.1 to 1 T are chosen (T = tesla). This leads to frequencies in the GHz region (centimetre waves).

What we have here described for a free electron is also valid for a free paramagnetic atom. In this case, the total resultant magnetic moment produced by the spin and orbital angular momenta of the atom, μ_j, must be used in (13.3 – 5).

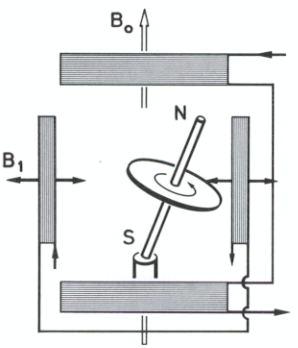

Fig. 13.2. Demonstration experiment for electron spin resonance: a gyroscope whose axle is a bar magnet is precessing in a magnetic field $\boldsymbol{B}_0$ (as well as in the gravitational field of the earth). The inclination of the axis of the gyroscope relative to $\boldsymbol{B}_0$ may be changed by means of an oscillating field $\boldsymbol{B}_1$ if the frequency of $\boldsymbol{B}_1$ is equal to the precession frequency of the gyroscope. For a lecture demonstration, it is expedient to construct the gyroscope in such a way that it is driven from the support pedestal S, for example using compressed air and following the principle of a water turbine

The fundamental idea of ESR may be illustrated by a mechanical model (Fig. 13.2): a gyroscope containing a bar magnet in its axis is precessing in a magnetic field. The precession frequency is (neglecting gravitational force)

$$\omega_L = \frac{|\boldsymbol{\mu}| \cdot |\boldsymbol{B}_0|}{|\boldsymbol{L}|}, \tag{13.6}$$

where $\boldsymbol{\mu}$ is the magnetic moment of the bar magnet and $\boldsymbol{L}$ is the angular momentum of the gyroscope.

The precession frequency or better, angular velocity ω_L of a magnetic gyroscope in a magnetic field is independent of the angle α between $\boldsymbol{\mu}$ and $\boldsymbol{B}_0$, since the torque produced by the field and the rate of change of the angular momentum vector both depend in the same way on the sine of the angle α (12.12). When gravitational force is neglected, the frequency ω_L is determined only by the magnetic moment $\boldsymbol{\mu}$ and the angular momentum $\boldsymbol{L}$ of the gyroscope, as well as by the torque produced by the field $\boldsymbol{B}_0$.

When we now let an additional oscillating field $\boldsymbol{B}_1$ with the frequency ω act perpendicular to $\boldsymbol{B}_0$, we observe a continuous increase or decrease in the angle of inclination α, depending on whether the field is in phase or out of phase with the motion of the gyroscope, provided that the frequency ω is equal to ω_L.

This model may be immediately transferred to the atom. We replace the magnetic moment of the bar magnet by the moment of the atom and obtain for the circular frequency of the electron spin resonance the following condition:

$$\omega_L = \frac{|\boldsymbol{\mu}| \cdot |\boldsymbol{B}_0|}{|\boldsymbol{l}|} = \gamma B_0 . \tag{13.7}$$

This is the Larmor frequency, which was already introduced in Sect. 12.3.

In the classical gyroscope model, the tip of the gyroscope axle moves on a spiral orbit from one stable position to another. This picture may be applied with considerable accuracy to the motion of the spin or the orbital angular momentum in an atom. There is an additional possibility for picturing the resonant transitions, which makes use of the fact that the spin or the angular momentum of an atom has only certain discrete allowed stationary orientations in a constant magnetic field $\boldsymbol{B}_0$. In this picture, the spin makes transitions between these discrete energy levels under the influence of the oscillating field $\boldsymbol{B}_1$. In particular, this means in the case of spin 1/2 that the spin flips from the one possible orientation to the other when the resonance condition (13.7) is fulfilled.

Electron spin resonance was observed for the first time in 1944 by the Russian physicist *Zavoisky*. The analogous spin resonance of paramagnetic atomic *nuclei* is seen under otherwise identical conditions at a frequency which is 3 orders of magnitude smaller, due to the fact that nuclear moments are about a factor of 1000 smaller than atomic magnetic moments; the corresponding frequencies are in the radio frequency region. This *nuclear magnetic resonance* (NMR) was observed in the solid state for the first time in 1946 by *Bloch* and *Purcell*, nearly 10 years after it had first been used by *Rabi* to measure the gyromagnetic ratio of nuclei in gas atoms (cf. Sect. 20.6).

A schematic of an ESR apparatus is shown in Fig. 13.3. Today, ESR spectrometers count as standard spectroscopic accessories in many physical and chemical laboratories. For technical reasons, usually a fixed frequency is used in the spectrometers;

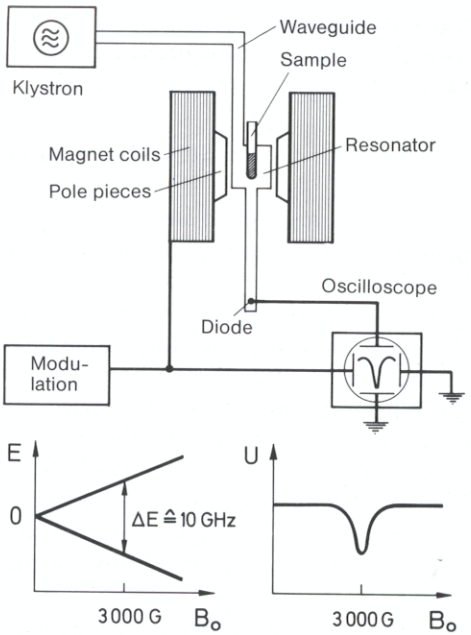

Fig. 13.3. Electron spin resonance. *Above:* Schematic representation of the experimental setup. The sample is located in a resonant cavity between the pole pieces of an electromagnet. The microwaves are generated by a klystron and detected by a diode. To increase the sensitivity of detection, the field $\boldsymbol{B}_0$ is modulated. *Below, left:* Energy states of a free electron as functions of the applied magnetic field. *Below, right:* Signal U from the diode as a function of B_0 for resonance

the magnetic field is varied to fulfil the resonance condition and obtain ESR transitions in absorption and sometimes in emission. The sample is usually placed in a microwave resonator; a frequently used wavelength is 3 cm (the so-called X-band). The microwave radiation is generated by a klystron and detected by a high frequency diode or a bolometer.

ESR is utilised for

- precision determinations of the gyromagnetic ratio and the g factor of the electron;
- measurement of the g factor of atoms in the ground state and in excited states for the purpose of analysing the term diagram;
- the study of various kinds of paramagnetic states and centres in solid state physics and in chemistry: molecular radicals, conduction electrons, paramagnetic ions in ionic and metallic crystals, colour centres.

The full importance of ESR will only become clear after we have treated the topic of hyperfine structure, i.e. when we discuss the interaction of the electronic spin with the spins of the neighbouring nuclei. Using this interaction, termed hyperfine splitting (Chap. 20), one can determine the spatial distribution of the electrons in molecules, in liquids, and in solids. More information about ESR and its significance for the physics of atoms, molecules, and solids is given in H. Haken and H. C. Wolf: *Molecular Physics and Elements of Quantum Chemistry*, Chap. 19.

13.3 The Zeeman Effect

13.3.1 Experiments

The splitting of the energy terms of atoms in a magnetic field can also be observed as a splitting of the frequencies of transitions in the optical spectra (or as a shift). A splitting of this type of spectral lines in a magnetic field was observed for the first time in 1896

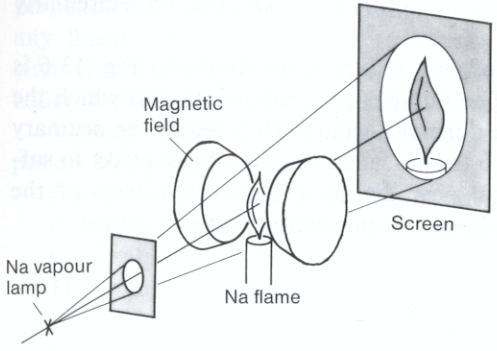

Fig. 13.4. Demonstration experiment for the Zeeman effect. A flame coloured with sodium or NaCl appears dark when projected using light from a Na vapour lamp. Upon switching on a magnetic field, it brightens, since the resonance between the light from the lamp and the light of the sodium flame is destroyed by the Zeeman effect. The wavelength of the light from the flame is shifted slightly by the magnetic field; this suffices to remove the resonance

by *Zeeman*. The effect is small; for its observation, spectral apparatus of very high resolution is required. These are either diffraction grating spectrometers with long focal lengths and a large number of lines per cm in the grating, or else interference spectrometers, mainly Fabry-Perot interferometers. We shall discuss this topic in more detail in Chap. 22.

There is, however, a simple lecture demonstration (Fig. 13.4) which shows the shift of the spectral lines in a magnetic field in a drastic manner: a flame, coloured yellow with sodium, is opaque to the yellow light of a sodium vapour lamp, because the latter represents resonance light, i.e. light whose wavelength matches the absorption and emission wavelength in the flame. If, however, a magnetic field is applied to the flame, the resonance between the light source (Na lamp) and the absorber (Na flame) is destroyed. On the observation screen, the previously "dark" flame brightens, because it has now become transparent to the light from the Na vapour lamp.

With a Fabry-Perot interferometer or with a grating spectrometer of sufficient resolution, the splitting in magnetic fields may be quantitatively measured. The splitting behaviour observed in moderate magnetic fields is illustrated in Figs. 13.5 and 13.6. The splitting of the cadmium line in Fig. 13.5 is called the "ordinary" Zeeman effect; using transverse observation (i.e. observation perpendicular to the direction of the applied magnetic field, Fig. 13.7), one sees the unshifted line as well as two symmetrically split components, each linearly polarised. With longitudinal observation

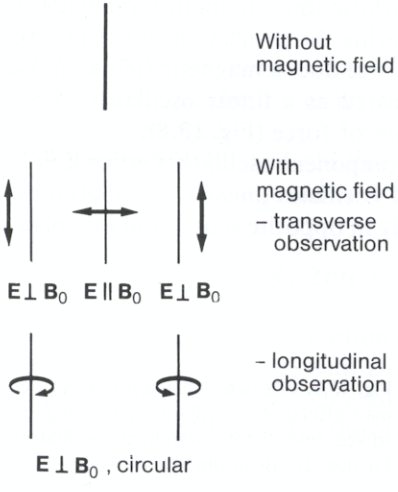

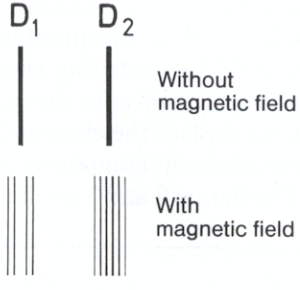

Fig. 13.6. Anomalous Zeeman effect, here using the sodium D lines. The D_1 line splits into four components, the D_2 line into six in a magnetic field. The wavelengths of the D_1 and D_2 lines are 5896 and 5889 Å; the quantum energy increases to the right in the diagram

Fig. 13.5. Ordinary Zeeman effect, e.g. for the atomic Cd line at $\lambda = 6438$ Å. With transverse observation the original line and two symmetrically shifted components are seen. Under longitudinal observation, only the split components are seen. The polarisation (E vector) is indicated

(parallel to the field lines), only the two shifted components are seen; they are circularly polarised in this case.

The splitting behaviour of the D lines of the sodium atom shown in Fig. 13.6 is typical of the *anomalous* Zeeman effect. The number of components into which the spectral lines are split is greater than in the normal Zeeman effect. Both the ordinary and the anomalous Zeeman effects merge to the so-called Paschen-Back effect in sufficiently large magnetic fields $\boldsymbol{B}_0$. We shall now discuss these three effects of the influence of magnetic fields on the spectral lines and the energy terms of atoms.

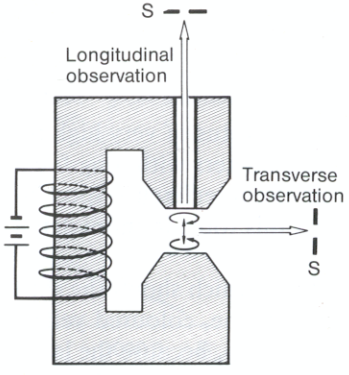

Fig. 13.7. Transverse and longitudinal observation of spectral lines in a magnetic field. The three component electrons used in the classical description of the Zeeman effect are indicated (orbits with arrows in the pole gap of the magnet). The emission of a light source in the magnetic field is observed either transversely or longitudinally (through a hole drilled in the magnet pole piece). S is the entrance slit of a spectrometer

13.3.2 Explanation of the Zeeman Effect from the Standpoint of Classical Electron Theory

The Zeeman effect may be understood to a large extent using classical electron theory, as was shown by *Lorentz* shortly after its discovery. We shall restrict ourselves to the ordinary Zeeman effect – the splitting of states with pure orbital angular momentum. If the resultant angular momentum is composed of both spin and orbital contributions, one speaks of the anomalous Zeeman effect. The normal Zeeman effect describes states in which no spin magnetism occurs. In these states, at least two electrons contribute in such a way that their spins are coupled to zero. Therefore, the normal Zeeman effect is found only for states involving several (at least two) electrons, which are treated in Chap. 17.

We discuss the emission of light by an electron whose motion about the nucleus is interpreted as an oscillation, for example by considering the projection of the motion on a certain direction. We ask the question, "What force does a magnetic field exert on a radiating electron?" The radiating electron is treated as a linear oscillator with a random orientation with respect to the magnetic lines of force (Fig. 13.8).

In the model, we replace the electron by three component oscillators according to the rules of vector addition: component oscillator 1 oscillates linearly, parallel to the direction of $\boldsymbol{B}_0$. Oscillators 2 and 3 oscillate circularly in opposite senses and in a plane

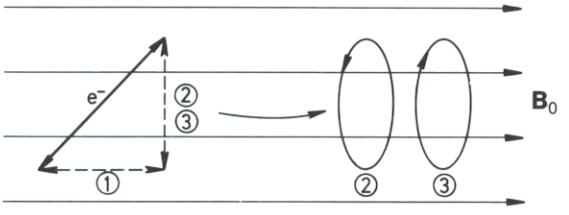

Fig. 13.8. Classical explanation of the Zeeman effect. An oscillating electron is resolved into three component oscillators. Further details in the text

perpendicular to the direction of $\boldsymbol{B}_0$. This resolution into components is allowed, since any linear oscillation may be represented by the addition of two counterrotating circular ones. Without the field $\boldsymbol{B}_0$, the frequency of all the component oscillators is equal to that of the original electron, namely ω_0.

We now inquire as to the forces which the magnetic field exerts on our three component electron-oscillators:

- Component 1, parallel to $\boldsymbol{B}_0$, experiences no force. Its frequency remains unchanged; it emits light which is linearly polarised with its $\boldsymbol{E}$ vector parallel to the vector $\boldsymbol{B}_0$.
- The circularly oscillating components 2 and 3 are accelerated or slowed down by the effect of magnetic induction on turning on the field $\boldsymbol{B}_0$, depending on their directions of motion. Their circular frequencies are increased or decreased by an amount

$$\delta\omega = \tfrac{1}{2}(e/m_0)B_0 = (\mu_B/\hbar)B_0 . \tag{13.8}$$

This is almost the same expression as that which we have already come to know as the Larmor frequency. It differs from the Larmor frequency only by a factor 2, because we are here dealing with an orbital moment ($g = 1$) instead of a spin moment ($g = 2$) as in the case of the Larmor frequency, which applies to electron spin resonance.

Classically, one can calculate the frequency shift $\delta\omega$ for the component oscillators as follows: without the applied magnetic field, the circular frequency of the component electrons is ω_0. The Coulomb force and the centrifugal force are in balance, i.e.

$$m\omega_0^2 \boldsymbol{r} = \frac{Ze^2}{4\pi\varepsilon_0 r^3}\boldsymbol{r} .$$

In a homogeneous magnetic field $\boldsymbol{B}_0$ applied in the z direction, the Lorentz force acts in addition; in Cartesian coordinates, the following equations of motion are then valid:

$$m\ddot{x} + m\omega_0^2 x - e\dot{y}B_0 = 0 , \tag{13.9a}$$

$$m\ddot{y} + m\omega_0^2 y + e\dot{x}B_0 = 0 , \tag{13.9b}$$

$$m\ddot{z} + m\omega_0^2 z = 0 . \tag{13.9c}$$

From (13.9c), we immediately find the solution for component oscillator 1, $z = z_0 \exp(\mathrm{i}\omega_0 t)$, i.e. the frequency of the electron which is oscillating in the z direction remains unchanged.

To solve (13.9a) and (13.9b), we substitute $u = x + \mathrm{i}y$ and $v = x - \mathrm{i}y$. It is easy to show that the equations have the following solutions (with the condition $eB_0/2m \ll \omega_0$):

$$u = u_0 \exp[\mathrm{i}(\omega_0 - eB_0/2m)t] \quad \text{and} \quad v = v_0 \exp[\mathrm{i}(\omega_0 + eB_0/2m)t] .$$

These are the equations of motion for a left-hand and a right-hand circular motion with the frequencies $\omega_0 \pm \delta\omega$, with $\delta\omega = eB_0/2m$. The component electron oscillators 2 and 3 thus emit or absorb circularly polarised light with the frequency $\omega_0 \pm \delta\omega$.

The splitting observed in the ordinary Zeeman effect is therefore correctly predicted in a classical model.

The frequency change has the magnitude:

$$\delta\nu = \delta\omega/2\pi = \frac{1}{4\pi}\,\frac{e}{m_0}B_0\,. \tag{13.10}$$

For a magnetic field strength $B_0 = 1\,\mathrm{T}$, this yields the value

$$\delta\nu = 1.4\cdot 10^{10}\,\mathrm{s}^{-1} \triangleq 0.465\,\mathrm{cm}^{-1}\,. \tag{13.11}$$

Independently of the frequency ν, we obtain the same frequency shift $\delta\nu$ for each spectral line with a given magnetic field B_0. Theory and experiment agree completely here. For the polarisation of the Zeeman components, we find the following predictions: component electron oscillator 1 has the radiation characteristics of a Hertzian dipole oscillator, oscillating in a direction parallel to $\boldsymbol{B}_0$. In particular, the $\boldsymbol{E}$ vector of the emitted radiation oscillates parallel to $\boldsymbol{B}_0$, and the intensity of the radiation is zero in the direction of $\boldsymbol{B}_0$. This corresponds exactly to the experimental results for the unshifted Zeeman component; it is also called the π component (π for parallel). If the radiation from the component electron oscillators 2 and 3 is observed in the direction of $\boldsymbol{B}_0$, it is found to be circularly polarised; observed in the direction perpendicular to $\boldsymbol{B}_0$, it is linearly polarised. This is also in agreement with the results of experiment. This radiation is called σ^+ and σ^- light, were σ stands for perpendicular (German "senkrecht") and the + and − signs for an increase or a decrease of the frequency. The σ^+ light is right-circular polarised, the σ^- light is left-circular polarised. The direction is defined relative to the lines of force of the $\boldsymbol{B}_0$ field, *not* relative to the propagation direction of the light.

The differing polarisations of the Zeeman components are used in optical pumping. In this technique, the exciting light can be polarised so as to populate individual Zeeman levels selectively, and thus to produce a spin orientation. More about this in Sect. 13.5.

13.3.3 Description of the Ordinary Zeeman Effect by the Vector Model

In the preceding section, we gave a purely classical treatment of the ordinary Zeeman effect; we now take the first step towards a quantum mechanical description. For this pupose, we employ the vector model which has been already introduced in Sect. 12.2 (cf. Fig. 13.9 and 13.11. Note that this figure illustrates the somewhat more complex case in which both orbital *and* spin magnetism play a rôle). A complete quantum mechanical treatment will be given in Chap. 14. The angular momentum vector $\boldsymbol{j}$ and the magnetic moment $\boldsymbol{\mu}_j$, which is coupled to $\boldsymbol{j}$, precess together around the field axis $\boldsymbol{B}_0$. The additional energy of the atom due to the magnetic field is then (Chap. 12 and Fig. 13.9 and 13.11)

$$V_{m_j} = -(\bar{\mu}_j)_z\cdot B_0 = +m_j g_j \mu_B B_0 \quad \text{with} \quad m_j = j,\, j-1,\ldots -j\ . \tag{13.12}$$

Here the factor g_l in (12.10) was replaced by g_j, because the total angular momentum is being considered.

The $(2j+1)$-fold directional degeneracy is thus lifted, and the term is split into $2j+1$ components. These are energetically equidistant. The distance between two components with $\Delta m_j = 1$ is

$$\Delta E = g_j \mu_B B_0\,.$$

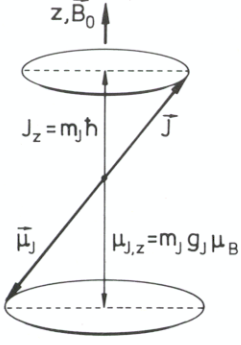

Fig. 13.9. Precession of $\boldsymbol{J}$ and $\boldsymbol{\mu}_J$ about the direction of the applied field $\boldsymbol{B}_0$: ordinary Zeeman effect, i.e., $\boldsymbol{J} = \boldsymbol{L}$

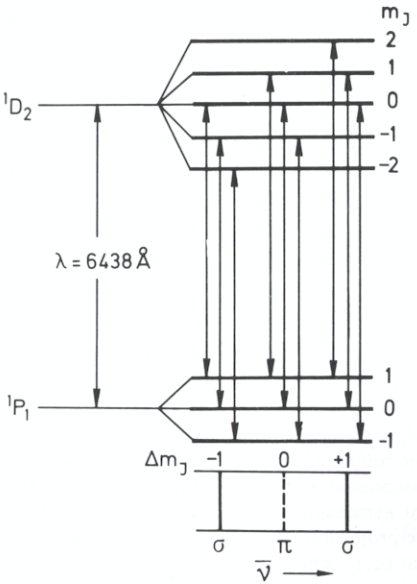

Fig. 13.10. Ordinary Zeeman effect. Splitting of the $\lambda = 6438$ Å line of the neutral Cd atom, transition $^1P_1 - {}^1D_2$, into three components. The transitions with $\Delta m_J = 0$ are called π transitions; those with $\Delta m_J = \pm 1$ are σ transitions. The quantum number J is written as a capital letter because the atom has several electrons (see Chap. 17). Here, $S = 0$, and $\boldsymbol{J} = \boldsymbol{L}$: we are dealing with a case of purely orbital magnetism

If we ignore the spin and consider only orbital magnetism (i.e. the ordinary Zeeman effect), g_j has a numerical value of 1 and we obtain

$$\delta\nu = \frac{1}{4\pi}\,\frac{e}{m_0}\,B_0\,. \tag{13.13}$$

The magnitude of the splitting is thus the same as in classical theory. For optical transitions, one must also make use of the selection rule

$$\Delta m_j = 0, \pm 1\,.$$

One thus obtains from quantum theory, too, the result that the number of lines is always three: the ordinary Zeeman triplet.

As an example, Fig. 13.10 shows the splitting diagram for a cadmium line. We must point out that the orbital angular momentum for the states of the Cd atom comprises the orbital angular momenta of two electrons, and is therefore indicated by a capital letter L. The spins of the two electrons are antiparallel and thus compensate each other, giving a total spin $S = 0$. Transitions between the components of different terms (e.g. $^1P_1$ or $^1D_2$ in Fig. 13.10) with the same Δm_j are energetically the same. The splitting is equal in each case because only orbital magnetism is involved. [See the discussion of the Landé g factor in Sect. 13.3.5, especially (13.18).] The undisplaced line corresponds to transitions with $\Delta m = 0$, while the displaced lines are the transitions with $\Delta m = \pm 1$. They are circularly polarised.

Polarisation and ordinary Zeeman splitting are a good example of the correspondence principle (Sect. 8.11). Based on the conservation of angular momentum for the system of electrons and light quanta, the polarisation behaviour of the Zeeman effect implies that light quanta have the angular momentum $1 \cdot \hbar$.

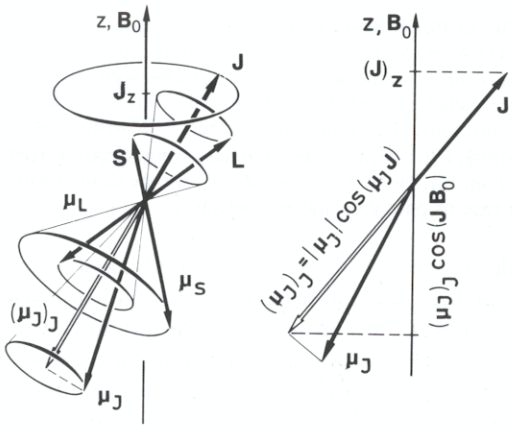

Fig. 13.11. *Left:* The relation between the angular momentum J, the magnetic moment μ_J and their orientation with respect to the magnetic field B_0 for strong spin-orbit coupling, cf. also Fig. 13.13. The angular momentum vectors S and L combine to form J. Likewise, the associated magnetic moments μ_L and μ_S combine to μ_J. Because spin and orbital magnetism have different gyromagnetic ratios, the directions of the vectors J and μ_J do not coincide. What can be observed is the projection of μ_J on J, as the time average of many precession cycles. That is, one observes the component $(\mu_J)_J$, which is therefore represented as $\bar{\mu}_J$ or $\bar{\mu}_S$, see the right-hand diagram. In the one-electron system, lower case letters can be used instead of S, L and J, as is done in the text. *Right:* The projection of μ_J on the vector J is $(\mu_J)_J$, see Fig. 13.14. The projection of $(\mu_J)_J$ on B_0 is calculated using the Landé factor. Because the angular momenta S and L are strongly coupled, the vector μ_J precesses rapidly around the negative extension of the vector J. Only the time average $(\mu_J)_J$ in the J direction can be observed. This precesses slowly, because of weak coupling, around the axis of B_0. The magnetic energy is the product of the field strength B_0 and the component of $(\mu_J)_J$ in the direction of B_0, i.e. $(\mu_J)_{J,z}$ or $(\bar{\mu}_J)_z \cdot B_0$. Lower case letters can be used instead of S, L, J in the one electron system.

Figure 13.11 illustrates the anomalous Zeeman effect (Sect. 13.3.4). The ordinary Zeeman effect (Sect. 13.3.3) is more simple. From $S = 0$ follows $\mu_J = \mu_L$, and the directions of the vectors $-\mu_J$ and $J = L$ coincide; see Fig. 13.9

13.3.4 The Anomalous Zeeman Effect

One speaks of the anomalous Zeeman effect when the angular momentum and magnetic moment of the two terms between which an optical transition occurs cannot be described by just one of the two quantum numbers s or l (or S or L), but are determined by both. Refer also to Fig. 13.11. This is the general case, in which atomic magnetism is due to the superposition of spin and orbital magnetism. The term "anomalous" Zeeman effect is historical, and is actually contradictory, because this is the normal case.

In cases of the anomalous Zeeman effect, the two terms involved in the optical transition have different g factors, because the relative contributions of spin and orbital magnetism to the two states are different. The g factors are determined by the total angular momentum j and are therefore called g_j factors. The splitting of the terms in the ground and excited states is therefore different, in contrast to the situation in the normal Zeeman effect. This produces a larger number of spectral lines. The calculation of the g_j factors follows in Sect. 13.3.5.

We will use the Na D lines (Fig. 13.12) as an example for a discussion of the anomalous Zeeman effect.

For the three terms involved in the transitions which produce the Na D line, namely the $^2S_{1/2}$, the $^2P_{1/2}$ and the $^2P_{3/2}$, the magnetic moments in the direction of the field are

$$(\mu_j)_{j,z} = -m_j g_j \mu_B \ , \qquad (13.14)$$

and the magnetic energy is

$$V_{m_j} = -(\mu_j)_{j,z} B_0 \,. \tag{13.15}$$

The number of splitting components in the field is given by m_j and is again $2j+1$. The distance between the components with different values of m_j – the so-called Zeeman components – is no longer the same for all terms, but depends on the quantum numbers l, s, and j:

$$\Delta E_{m_j, m_{j-1}} = g_j \mu_B B_0 \,. \tag{13.16}$$

Experimentally, it is found that $g_j = 2$ for the ground state $^2S_{1/2}$, 2/3 for the state $^2P_{1/2}$ and 4/3 for the state $^2P_{3/2}$. We shall explain these g_j factors in the next section. For optical transitions, the selection rule is again $\Delta m_j = 0, \pm 1$. It yields the 10 lines shown in Fig. 13.12. The spectrum which is, in fact, observed is shown schematically in Fig. 13.13.

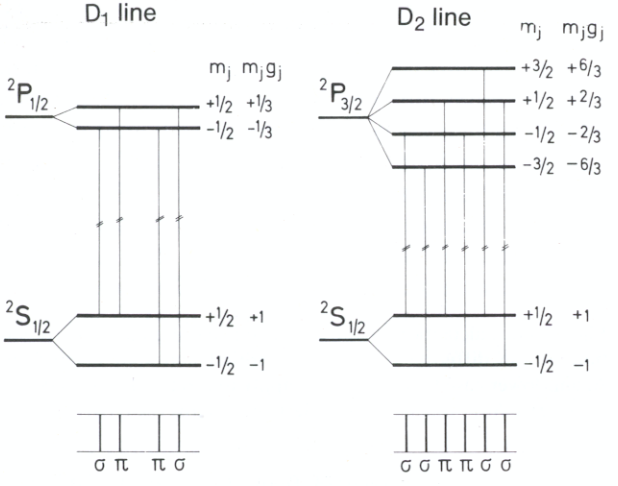

◀ **Fig. 13.12.** Anomalous Zeeman effect. Splitting of the D_1 and D_2 lines of the neutral Na atom, transitions $^2S_{1/2} - {}^2P_{1/2}$ and $^2S_{1/2} - {}^2P_{3/2}$, into 4 and 6 components, respectively, in a magnetic field. Here, $S=0$ and we are dealing with purely *orbital* magnetism. The $^2P_{3/2}$ state is higher in energy than the $^2P_{1/2}$ state; this is not shown in the figure. Compare also Fig. 12.18

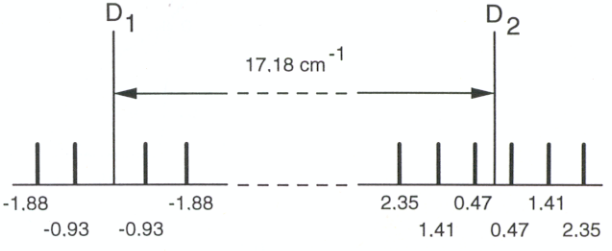

Fig. 13.13. Energy splitting (in cm^{-1}) of the D_1 and D_2 lines in a magnetic field of 3 T (Zeeman effect)

The significance of the Zeeman effect is primarily its contribution to empirical term analysis. Term splitting depends unequivocally on the quantum numbers l, s and j or, in many-electron atoms, L, S and J (Chap. 17). The quantum numbers can therefore be determined empirically from measurements of the Zeeman effect.

13.3.5 Magnetic Moments with Spin-Orbit Coupling

In anomalous Zeeman splitting, other values of g_j than 1 (orbital magnetism) or 2 (spin magnetism) are found. We can understand these quantitatively through the vector model.

The g_j factor links the magnitude of the magnetic moment of an atom to its total angular momentum. The magnetic moment is the vector sum of the orbital and spin magnetic moments,

$$\mu_j = \mu_s + \mu_l \,.$$

The directions of the vectors μ_l and l are antiparallel, as are those of the vectors μ_s and s. In contrast, the directions of j and $-\mu_j$ do not in general coincide. This is a result of the difference in the g factors for spin and orbital magnetism. This is demonstrated in Figs. 13.14 and 13.11.

The magnetic moment μ_j resulting from vector addition of μ_l and μ_s precesses around the total angular momentum vector j, the direction of which is fixed in space. Due to the strong coupling of the angular momenta, the precession is rapid. Therefore only the time average of its projection on j can be observed, since the other components cancel each other in time. This projection $(\mu_j)_j$ precesses in turn around the B_0 axis of the applied magnetic field B_0. In the calculation of the magnetic contribution to the energy V_{m_j}, the projection of μ_j on the j axis $(\mu_j)_j$ must therefore be inserted in (13.15). Its magnitude can be calculated from the vector model: from Figs. 13.11 and 13.14, the j component of μ_j is

$$|(\mu_j)_j| = |\mu_l|\cos(l,j) + |\mu_s|\cos(s,j)$$

$$= \mu_B[\sqrt{l(l+1)}\cos(l,j) + 2\sqrt{s(s+1)}\cos(s,j)] .$$

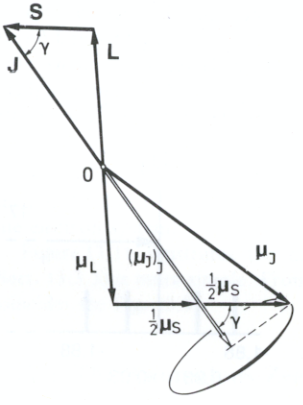

Fig. 13.14. Calculation of the J components of μ_J and interpretation of the differing g factors of orbital and spin magnetism. Again, lower case letters s, l and j apply to single-electron systems, upper case S, L and J to many-electron systems

The expressions for $\cos(l,j)$ and $\cos(s,j)$ are derived from Figs. 13.14 and 13.11 using the law of cosines. The length of the vectors is again $\sqrt{l(l+1)}\hbar$ or $\sqrt{s(s+1)}\hbar$, respectively. We shall present a deeper quantum theoretical justification for this in Sect. 14.3.

We then have for the magnitude of $(\mu_j)_j$,

$$|(\mu_j)_j| = \frac{3j(j+1)+s(s+1)-l(l+1)}{2\sqrt{j(j+1)}}\mu_B = g_j\sqrt{j(j+1)}\mu_B , \tag{13.17}$$

and for the moment

$$(\mu_j)_j = -g_j\mu_B j/\hbar$$

with

$$g_j = 1 + \frac{j(j+1)+s(s+1)-l(l+1)}{2j(j+1)} , \tag{13.18}$$

and for the component in the z direction,

$$(\mu_j)_{j,z} = -m_j g_j \mu_B . \tag{13.19}$$

The Landé factor g_j defined in this way has a numerical value of 1 for pure orbital magnetism ($s = 0$) and 2 (more exactly, 2.0023) for pure spin magnetism ($l = 0$). For mixed magnetism, one observes values which differ from these two cases. By making the appropriate substitutions, one can easily see that the g factors given in the preceding section for the terms of the sodium atom are obtained from (13.18). In many-electron atoms, the quantum numbers s, l and j are replaced by S, L and J, as already mentioned (but see Sect. 17.3.3). This has been done in Figs. 13.11 and 13.14.

13.4 The Paschen-Back Effect

The preceding considerations on the splitting of spectral lines in a magnetic field hold for "weak" magnetic fields. "Weak" means that the splitting of energy levels in the magnetic field is small compared to fine structure splitting; or, in other words, the coupling between the orbital and spin moments, the so-called spin-orbit coupling, is stronger than the coupling of either the spin or the orbital moment alone to the external magnetic field. Since spin-orbit coupling increases rapidly with increasing nuclear charge Z (Sect. 12.8), the conditions for a "strong" field are met at a much lower field with light atoms than with heavy atoms. For example, the spin-orbit splitting of the sodium D lines is 17.2 cm^{-1}, while the splitting for the corresponding lines of the lithium atom is 0.3 cm^{-1}. The Zeeman splitting in an external field B_0 of 30 kG (3 T) is the same in both cases, about 1 cm^{-1}, cf. Fig. 13.13. Thus this field is a "strong" magnetic field for lithium, but a "weak" field for sodium.

When the magnetic field $\boldsymbol{B}_0$ is strong enough so that the above condition is no longer fulfilled, the splitting picture is simplified. The magnetic field dissolves the fine structure coupling. $\boldsymbol{l}$ and $\boldsymbol{s}$ are, to a first approximation, uncoupled, and precess independently around $\boldsymbol{B}_0$. The quantum number for the total angular momentum, j, thus loses its meaning. This limiting case is called the Paschen-Back effect.

The components of the orbital and spin moments $(\mu_l)_z$ and $(\mu_s)_z$ in the field direction are now individually quantised. The corresponding magnetic energy is

$$V_{m_s, m_l} = (m_l + 2 m_s) \mu_B B_0 \tag{13.20}$$

and the splitting of the spectral lines is

$$\Delta E = (\Delta m_l + 2 \Delta m_s) \mu_B B_0 . \tag{13.21}$$

For optical transitions, there are again selection rules, and as before, $\Delta m_l = 0$ or ± 1 for π or σ transitions. Since electric dipole radiation cannot, to a first approximation, effect a spin flip, it also holds that $\Delta m_s = 0$. With these rules, (13.21) yields a triplet of spectral lines like those of the ordinary Zeeman effect.

Figure 13.15 shows the splitting scheme of the Na D lines. A vector model is shown in Fig. 13.16, which makes it clear that a total angular momentum vector $\boldsymbol{j}$ cannot even be defined here. Like the Zeeman effect, the Paschen-Back effect is chiefly used in

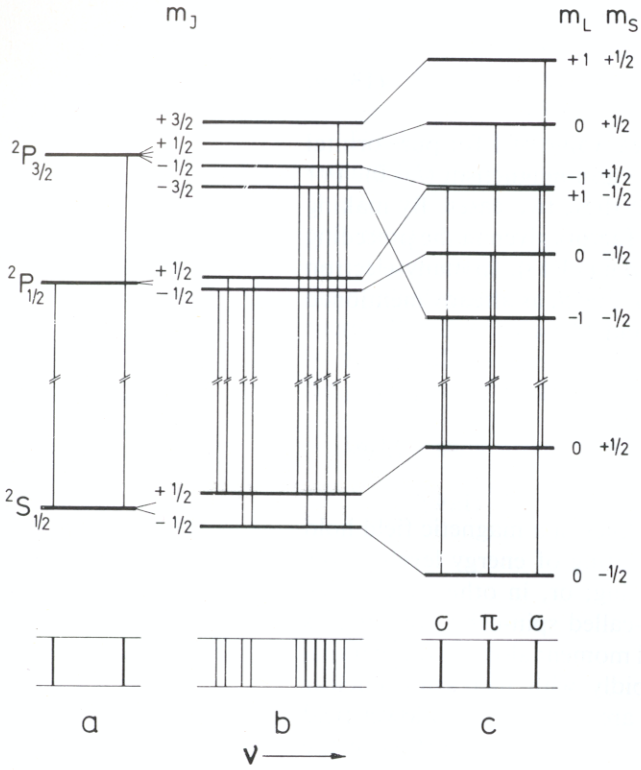

Fig. 13.15a – c. Paschen-Back effect (**c**) and Zeeman effect (**b**) with the D_1 and D_2 lines of the neutral sodium atom (**a**). In the limiting case of strong magnetic fields, one observes one unshifted and two symmetrically split lines, as in the ordinary Zeeman effect

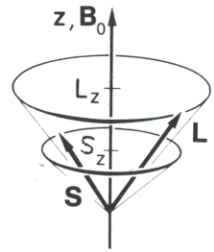

Fig. 13.16. Paschen-Back effect. In the limiting case of a strong magnetic field B_0, the spin S and orbital L angular momenta align independently with the field B_0. A total angular momentum J is not defined

empirical term analysis. In many-electron atoms, where the single-electron quantum numbers j, l, and s are replaced by the many-electron quantum numbers J, L and S, this method is especially important (Chap. 17).

The area between the limiting cases of weak fields (Zeeman effect) and strong fields (Paschen-Back effect) is difficult to analyse, both theoretically and experimentally.

13.5 Double Resonance and Optical Pumping

One can make use of the difference in polarisation of the various Zeeman components in order to populate selectively individual Zeeman levels, even when the spectral resolution is insufficient or the linewidth is too great to obtain the excited state otherwise. This is the simplest case of optical pumping.

The first experiment of this type is represented in Fig. 13.17 (*Brossel, Bitter* and *Kastler* 1949 – 1952). Mercury atoms in an external magnetic field $\boldsymbol{B}_0$ are excited by irradiation with linearly polarised light in a π transition to the $m_J = 0$ level of the $^3P_1$ excited state. The emission from these atoms is also linearly polarised π light. Now one can induce transitions $\Delta m = \pm 1$ with a high-frequency coil perpendicular to $\boldsymbol{B}_0$, as shown in Fig. 13.17, and thus populate the Zeeman substates $m = 1$ and $m = -1$. The light emitted from these levels, however, is circularly polarised σ light. The emission of circularly polarised light in a direction perpendicular to that of the π emission can thus be used for the detection and measurement of $\Delta m = \pm 1$ transitions between Zeeman substates.

Here, the same transitions as in electron spin resonance are observed, but they are detected optically. By means of this *double resonance technique* (double excitation with light and with high-frequency radiation), an extremely high detection sensitivity can be reached, because the high-frequency quanta with small quantum energies are detected via the much more energetic light quanta. In this way, the detection of spin resonance in a short-lived excited state becomes possible. Double resonance methods of this type have attained considerable importance in spectroscopy in the past 30 years.

The principle of *optical pumping* may be explained conveniently using the example of the sodium D lines, e.g. the transition from the $^2S_{1/2}$ ground state to the $^2P_{1/2}$ excited state. In an applied magnetic field, both terms are split into the Zeeman terms $m_j = \pm 1/2$ (Figs. 13.12 and 13.18). If the "pumping" light is now circularly polarised, for example as σ^+ light, only transitions from $m_j = -1/2$ in the ground state to the $m_j = +1/2$ excited state can take place, populating only the latter state. Emission from this state can occur either as σ^+ light, leading to the $^2S_{1/2}$, $m_j = -1/2$ initial state, or as π light, leading to the ground state term with $m_j = +1/2$. Overall, this *pumping cycle* increases the population of the terms with $m_j = +1/2$ in the ground state at the cost of those with $m_j = -1/2$. An equalisation of the populations can occur through *relaxation* processes, for example by means of collisions of the Na atoms with one another or

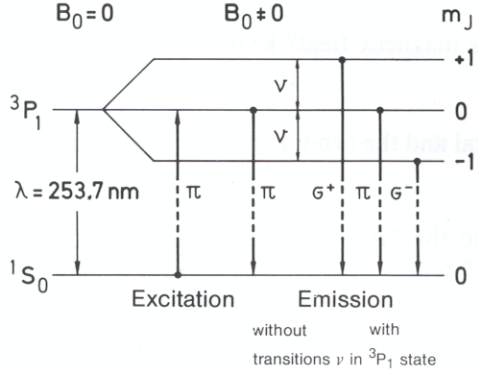

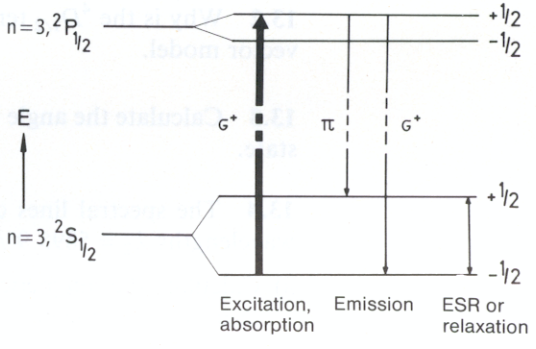

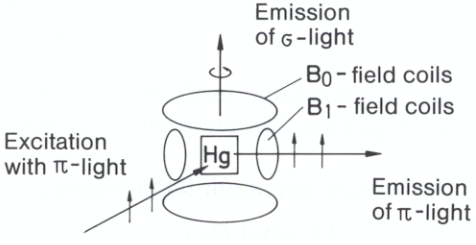

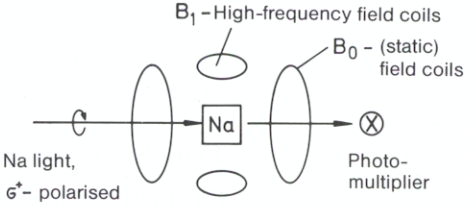

Fig. 13.17. Double resonance, after the method of *Brossel*, *Bitter* and *Kastler*. In the upper part of the figure, the three Zeeman levels of the excited state $^3P_1$ are shown. The lower part shows the experimental arrangement. The mercury atoms are contained in a cuvette between two pairs of coils, which produce the constant field $\boldsymbol{B}_0$ and the high-frequency field $\boldsymbol{B}_1$. The transition occurs between the ground state of the Hg atom $6s^2(^1S_0)$ and the excited state $6s6p(^3P_1)$

Fig. 13.18. Optical pumping of the transition $^2S_{1/2} - {}^2P_{1/2}$ of the sodium atom. In the field $\boldsymbol{B}_0$, the terms split up into Zeeman terms with $m_j = \pm 1/2$. Only atoms in the ground state $m_j = -1/2$ absorb the σ^+ light with which the sample is irradiated. π transitions occurring in emission from the excited state lead to an increase in the population of atoms in the ground state with $m_j = +1/2$. With the high-frequency field, transitions from $m_j = +1/2$ to $m_j = -1/2$ are induced, increasing the number of atoms which are able to absorb the pumping light

with the walls of the container. If these processes are not sufficiently rapid, one can induce transitions in the ground state by irradiation with microwaves. These electron spin resonance transitions change the populations of the Zeeman terms. The *detection* of this ESR can be accomplished *optically*, namely through the change in the intensity of the absorption from $^2S_{1/2}$, $m_j = -1/2$ to $^2P_{1/2}$, $m_j = +1/2$, provided that the population of the ground state terms was altered by optical pumping. Figure 13.18 shows the experimental arrangement schematically. This is thus also a double resonance method.

Double resonance methods, in which magnetic resonance transitions are detected by means of the absorption or emission of light in the visible or ultraviolet spectral ranges, have also acquired considerable importance in molecular and solid-state physics. They are termed ODMR, for *optically-detected magnetic resonance*. This subject is treated in more detail in *Molecular Physics and Quantum Chemistry* by H. Haken and H.C. Wolf, Sect. 19.7.

Problems

13.1 What frequency is required to induce electron spin transitions from the parallel to the antiparallel configuration, or vice versa, if the magnetic field is 10^{-1} tesla?

13.2 Why is the $^4D_{1/2}$ term not split in a magnetic field? Explain this in terms of the vector model.

13.3 Calculate the angle between the total and the orbital angular momenta in a $^4D_{3/2}$ state.

13.4 The spectral lines corresponding to the $3p \leftrightarrow 3s$ transition in sodium have the wavelengths $\lambda_2 = 5895.9$ Å and $\lambda_1 = 5889{,}6$ Å.

a) Calculate the magnetic field strength at which the lowest Zeeman level of the $^2P_{3/2}$ term would coincide with the highest level of the $^2P_{1/2}$ term, if the conditions for the anomalous Zeeman effect were still fulfilled.

b) How large are the frequency differences between the outer two components of the D_1 line and of the D_2 line in a magnetic field of 1 tesla?

13.5 Discuss the splitting of the lines in the $3d \leftrightarrow 2p$ transition in the presence of a magnetic field when the Zeeman splitting is small compared to the spin-orbit interaction.

13.6 Sketch the Zeeman splitting in the lines of the hydrogen atom Balmer series.

Calculate the magnetic moments of the states $P_{1/2}$, $P_{3/2}$, $D_{3/2}$ and $D_{5/2}$.

Also sketch the splitting in the Paschen-Back effect. At what magnetic field does the transition from the Zeeman to the Paschen-Back effect occur?

13.7 a) Consider hydrogen atoms in a magnetic field $B_0 = 4.5$ tesla. At this field strength, is the splitting of the H_α line ($n = 3 \rightarrow n = 2$) due to the anomalous Zeeman effect or the Paschen-Back effect? Support your answer. (The spin-orbit coupling between the $3^2P_{1/2}$ and $3^2P_{3/2}$ terms of the hydrogen atom is 0.108 cm^{-1}.)

b) Sketch the splitting of the energy levels in the given magnetic field and show the transitions which contribute to the H_α line. Into how many components is the H_α line split?

c) Determine the specific charge e/m of the electron, given that the frequency splitting between two neighbouring components is $6.29 \cdot 10^{10}$ Hz. The fine structure can be ignored here.

d) Is the wavelength splitting in the first line of the Lyman series ($n = 2 \rightarrow n = 1$) smaller, larger or the same as that of the H_α line?

13.8 a) Sketch the energy levels of a free electron in a magnetic field as a function of the field strength.

b) Consider two electrons whose spins are coupled (the precise coupling mechanism is not important for the problem; e.g. they could interact as two magnetic dipoles). How many possible orientations are there? Distinguish between singlet and triplet states.

c) What is the minimum number of electrons which you must couple together in order to produce a sextet state?

Hint: An x-tet state is named for its multiplicity.